

**Supplementary information**

---

**Principles of mitoribosomal small subunit assembly in eukaryotes**

---

In the format provided by the authors and unedited

## Supplementary Information

### Principles of mitoribosomal small subunit assembly in eukaryotes

Nathan J. Harper<sup>1,2,3</sup>, Chloe Burnside<sup>1,2,3</sup>, and Sebastian Klinge<sup>1,\*</sup>

<sup>1</sup> Laboratory of Protein and Nucleic Acid Chemistry, The Rockefeller University, New York, New York 10065, USA

<sup>2</sup> Tri-Institutional Training Program in Chemical Biology, The Rockefeller University, New York, New York 10065, USA

<sup>3</sup> These authors contributed equally to this work

\* Correspondence: [klinge@rockefeller.edu](mailto:klinge@rockefeller.edu) (S.K.)

## TABLE OF CONTENTS

Supplementary Fig. 1 - Uncropped gel images.

Supplementary Fig. 2 - Biallelic editing of human cell lines and human complex purification.

Supplementary Fig. 3 - Human METTL17 dataset cryo-EM data collection and analysis.

Supplementary Fig. 4 - Cryo-EM processing of human State A.

Supplementary Fig. 5 - Cryo-EM processing of human State B.

Supplementary Fig. 6 - Cryo-EM processing of human State C.

Supplementary Fig. 7 - Cryo-EM processing of human State D.

Supplementary Fig. 8 - Cryo-EM processing of human State E.

Supplementary Fig. 9 - Cryo-EM processing of human State C\*.

Supplementary Fig. 10 - Local resolution analysis of human State A.

Supplementary Fig. 11 - Local resolution analysis of human State B.

Supplementary Fig. 12 - Local resolution analysis of human State C.

Supplementary Fig. 13 - Local resolution analysis of human State D.

Supplementary Fig. 14 - Local resolution analysis of human State E.

Supplementary Fig. 15 - Local resolution analysis of human State C\*.

Supplementary Fig. 16 - Validation of composite maps for human States A and B.

Supplementary Fig. 17 - Validation of composite maps for human States C and D.

Supplementary Fig. 18 - Validation of composite maps for human States E and C\*.

Supplementary Fig. 19 - Representative cryo-EM densities and models for human structures.

Supplementary Fig. 20 - Purification of yeast mtSSU assembly intermediates.

Supplementary Fig. 21 - Initial cryo-EM processing of yeast Ccm1-containing particles.

Supplementary Fig. 22 - Cryo-EM processing of yeast States 1 and 2.

Supplementary Fig. 23 - Cryo-EM processing of yeast Rsm22-containing particles (State 3).

Supplementary Fig. 24 - Local resolution analysis of yeast reconstructions

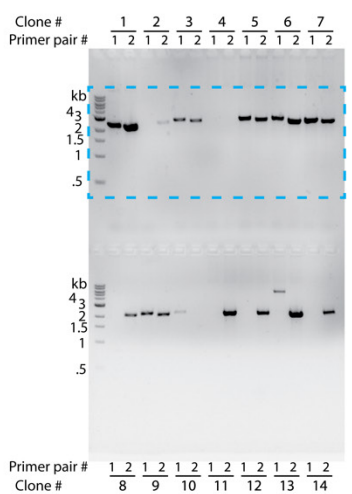
Supplementary Fig. 25 - Validation of composite maps for yeast States 1-3.

Supplementary Fig. 26 - Representative cryo-EM densities and models for yeast structures.

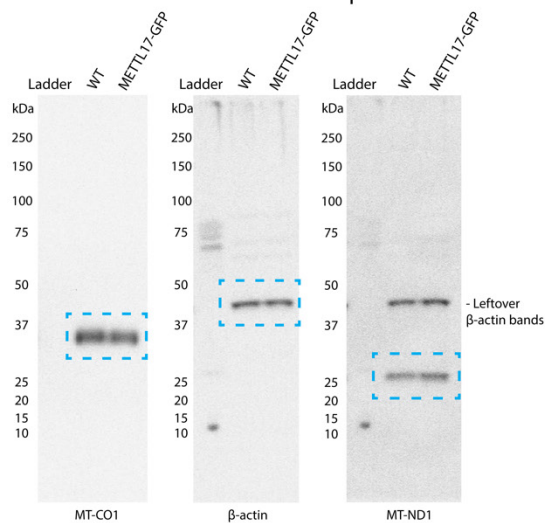
Supplementary Fig. 27 - Pet127 knockout results in accumulation of pre-15S rRNA and a decrease in bound assembly factors.

Supplementary References

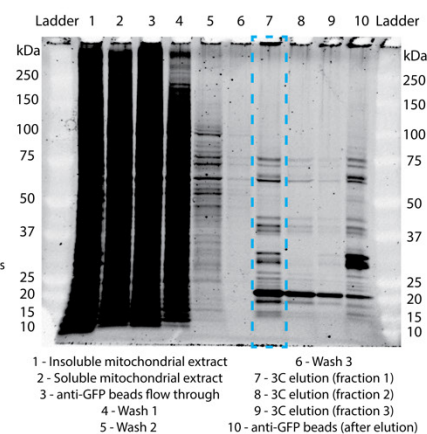
**a** METTL17 Genomic verification



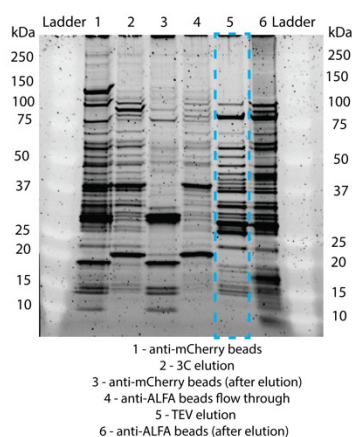
**b** METTL17-GFP OXPHOS subunit expression western blot



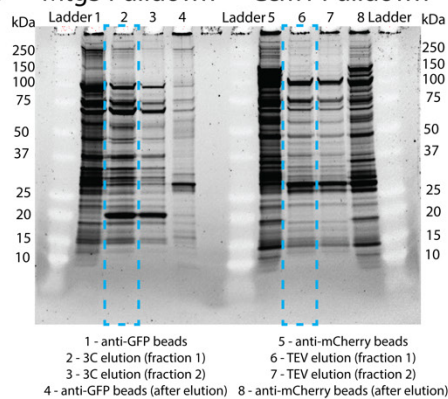
**c** METTL17 Pulldown



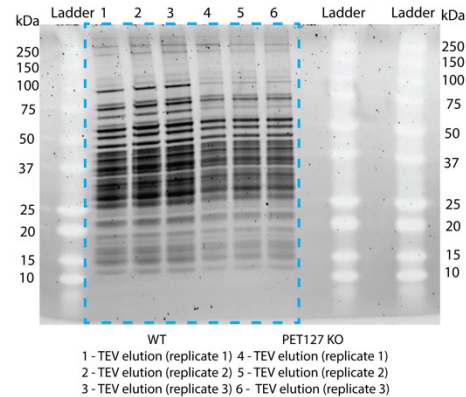
**d** Rsm22 Pulldown



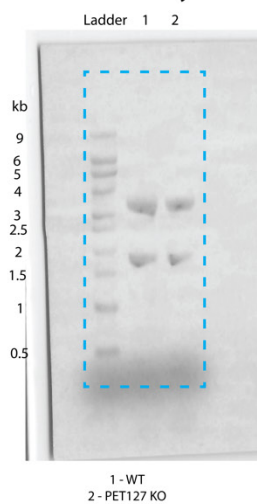
**e** Mtg3 Pulldown Ccm1 Pulldown



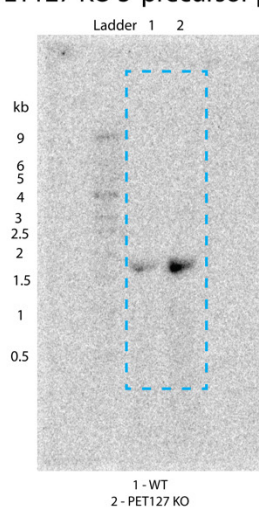
**f** PET127 KO IP



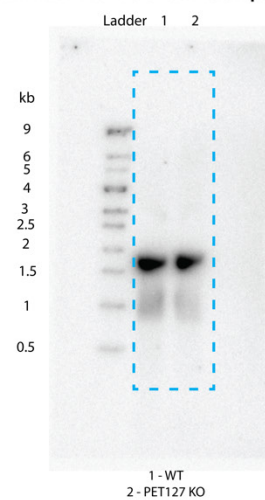
**g** PET127 KO Methylene Blue



**h** PET127 KO 5' precursor probe

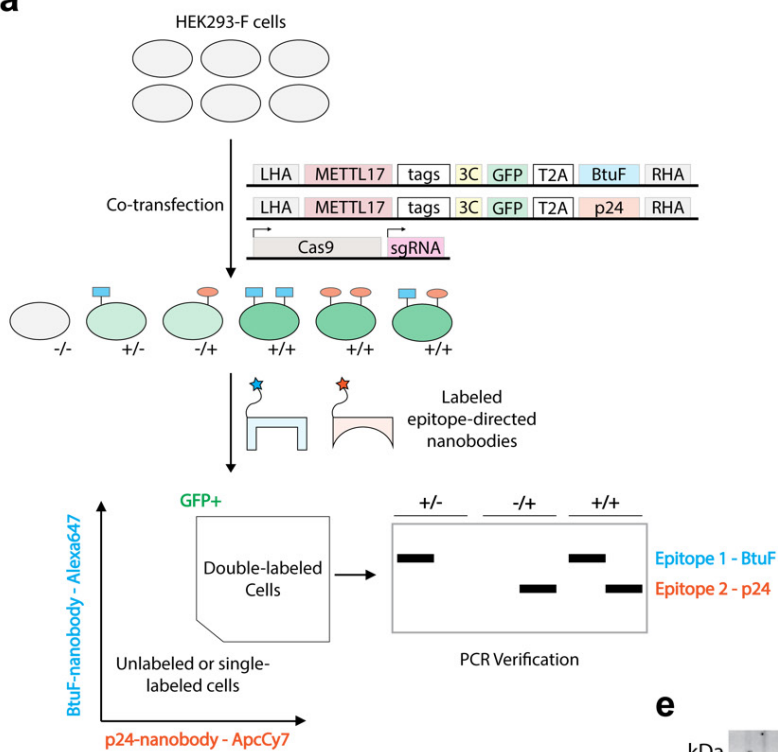
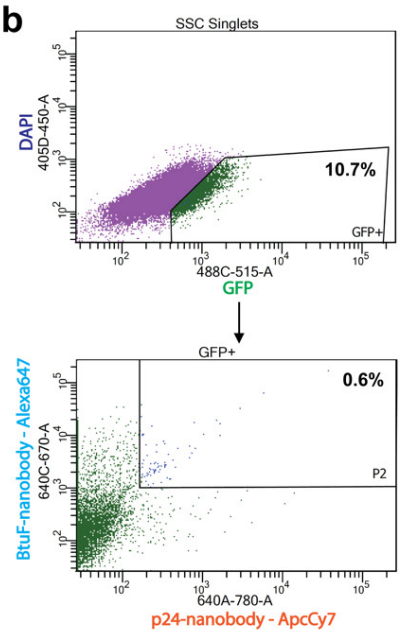
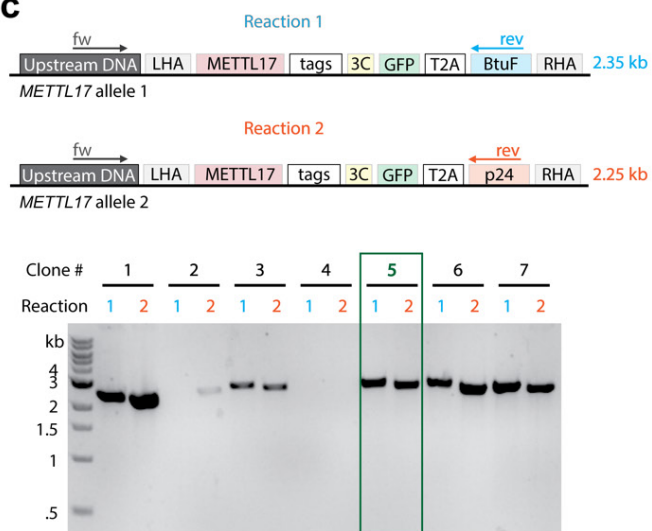
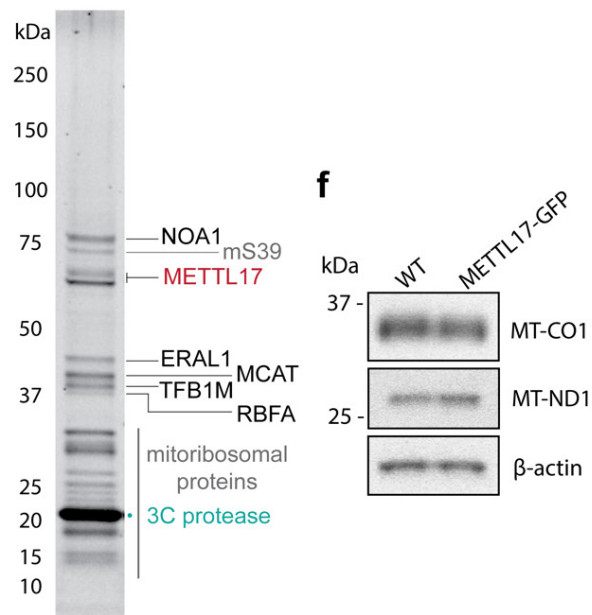
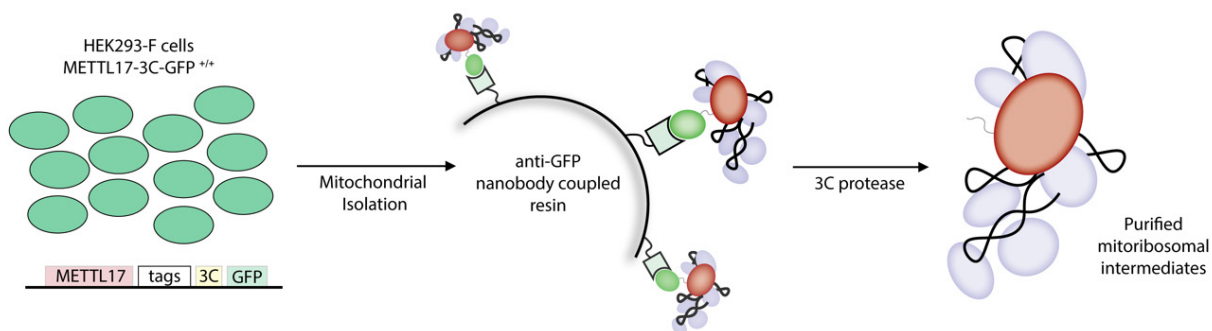


**i** PET127 KO 15S central probe



**Supplementary Fig. 1. Uncropped gel images.**

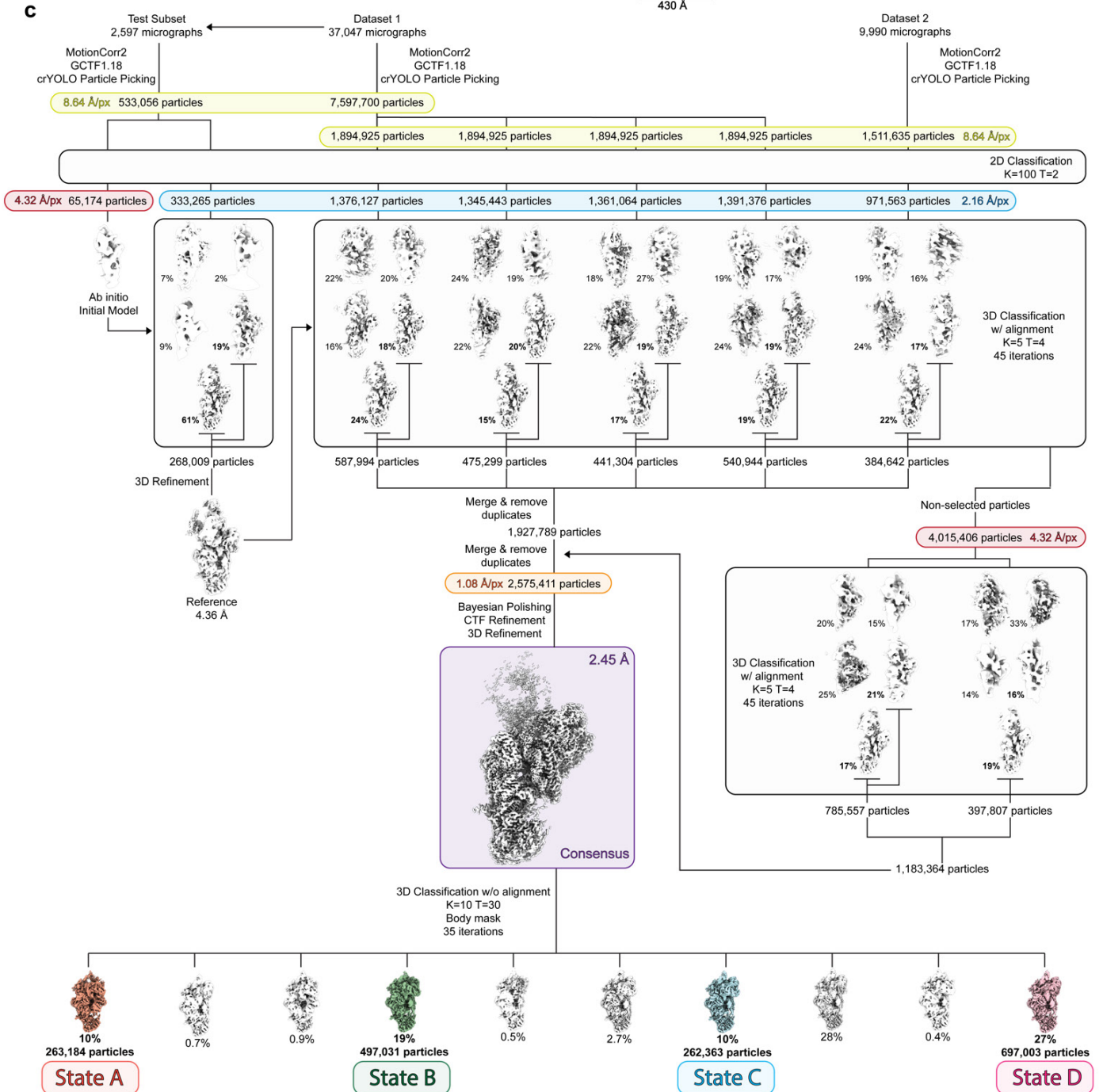
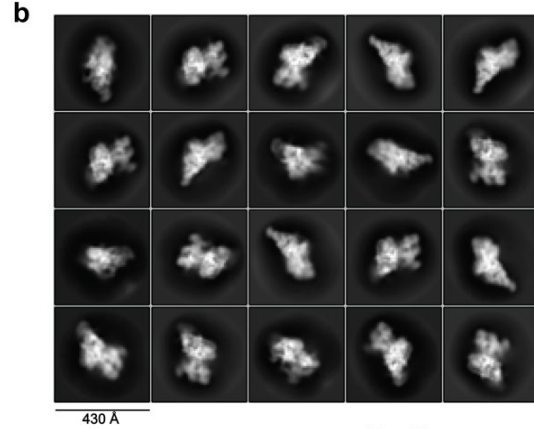
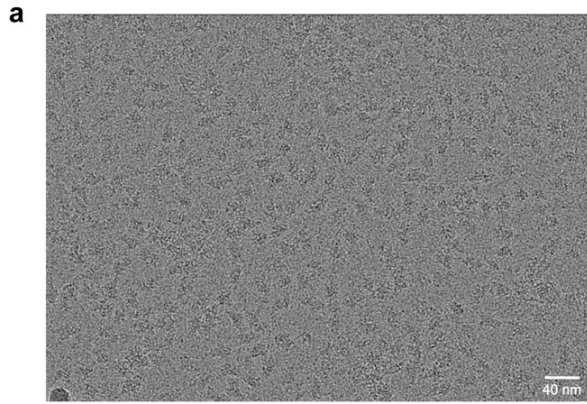
Uncropped gel images relating to: **(a)** Supplementary Fig. 2c, **(b)** Supplementary Fig. 2f, **(c)** Supplementary Fig. 2e, **(d)** Supplementary Fig. 20f, **(e)** Supplementary Fig. 20b,j, **(f)** Supplementary Fig. 27c, **(g-i)** Supplementary Fig. 27b. Blue dotted rectangles show approximate cropping dimensions used in related figures.

**a****b****c****e****d**

**Supplementary Fig. 2. Biallelic editing of human cell lines and human complex purification.**

(a) Simplified scheme of genomic editing using SNEAK-PEEC targeting METTL17. See methods for details. (b) FACS sorting on cells transfected with repair templates and SpCas9 targeting METTL17. Inset percentages denote proportion of cells positive for GFP (upper panel), and proportion of GFP positive cells with signal for both cell surface display epitopes (bottom panel). Cells from P2 were sorted to generate single cell clonal populations. (c) PCR verification of single cell clones from FACS sorting. Primer annealing locations are shown in genomic context in the upper panel. Samples were run on a 1% Agarose-TAE gel with EtBr. Highlighted clone was used for subsequent experiments. (d) Purification scheme for METTL17-containing mitoribosomal intermediates. (e) Representative SDS-PAGE gel of eluted sample. Proteins were identified with LC-MS/MS (Supplementary Data S1). Immunoprecipitation experiments were repeated at least 3 times with similar results. (f) Western blot showing unchanged expression of mitochondrially encoded OXPHOS subunits MT-CO1 and MT-ND1 in METTL17-GFP tagged cell line versus WT cells. The western blot was performed 3 times with similar results. For gel source data, see Supplementary Fig. 1.

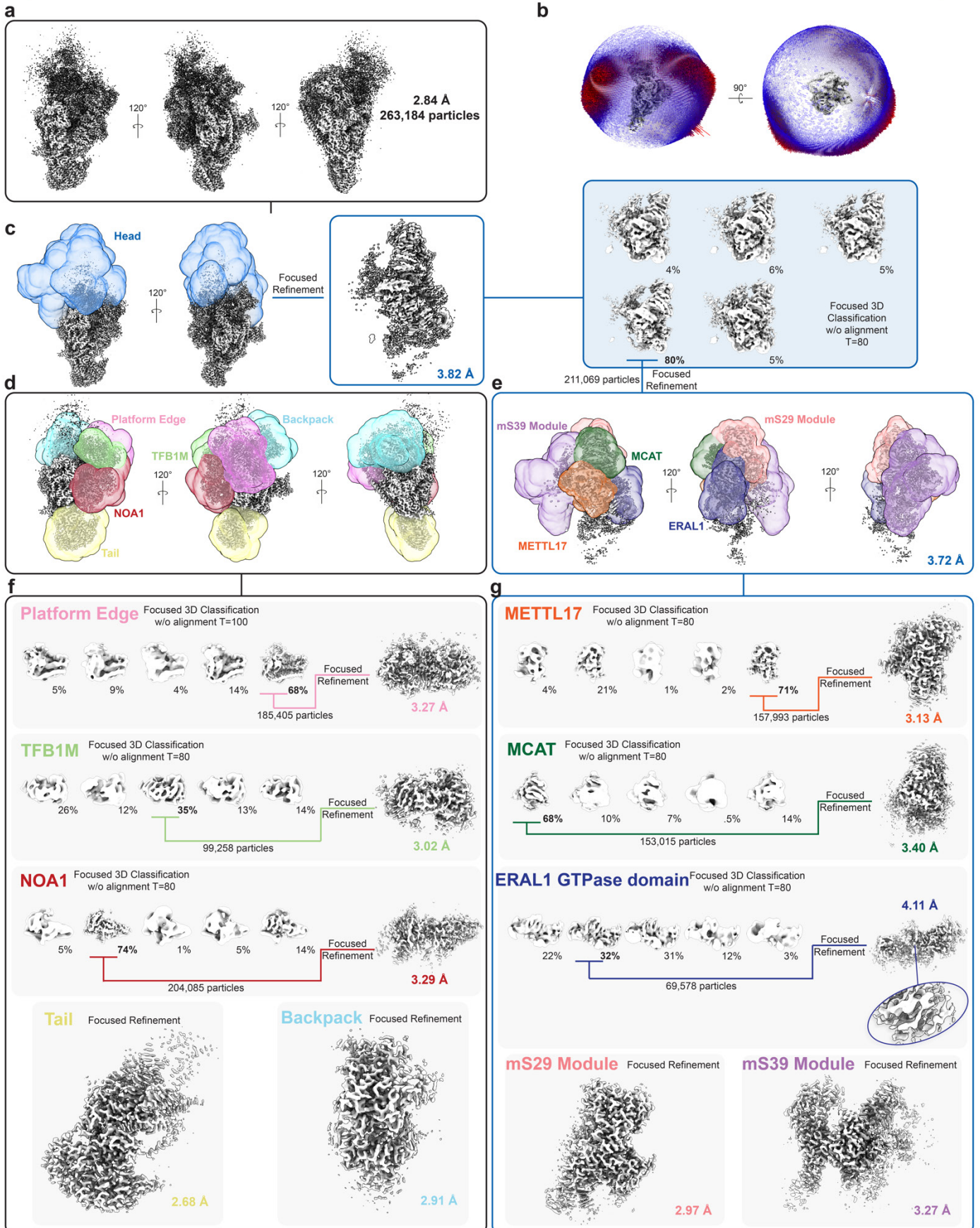




**Supplementary Fig. 3. Human METTL17 dataset cryo-EM data collection and analysis.**

(a) Motion corrected cryo-EM micrograph representative of 47,037 total micrographs. (b) 15 most populated 2D class averages (8x binned, 8.64 Å/px). (c) Initial data processing workflow and identification of 4 discrete assembly states.

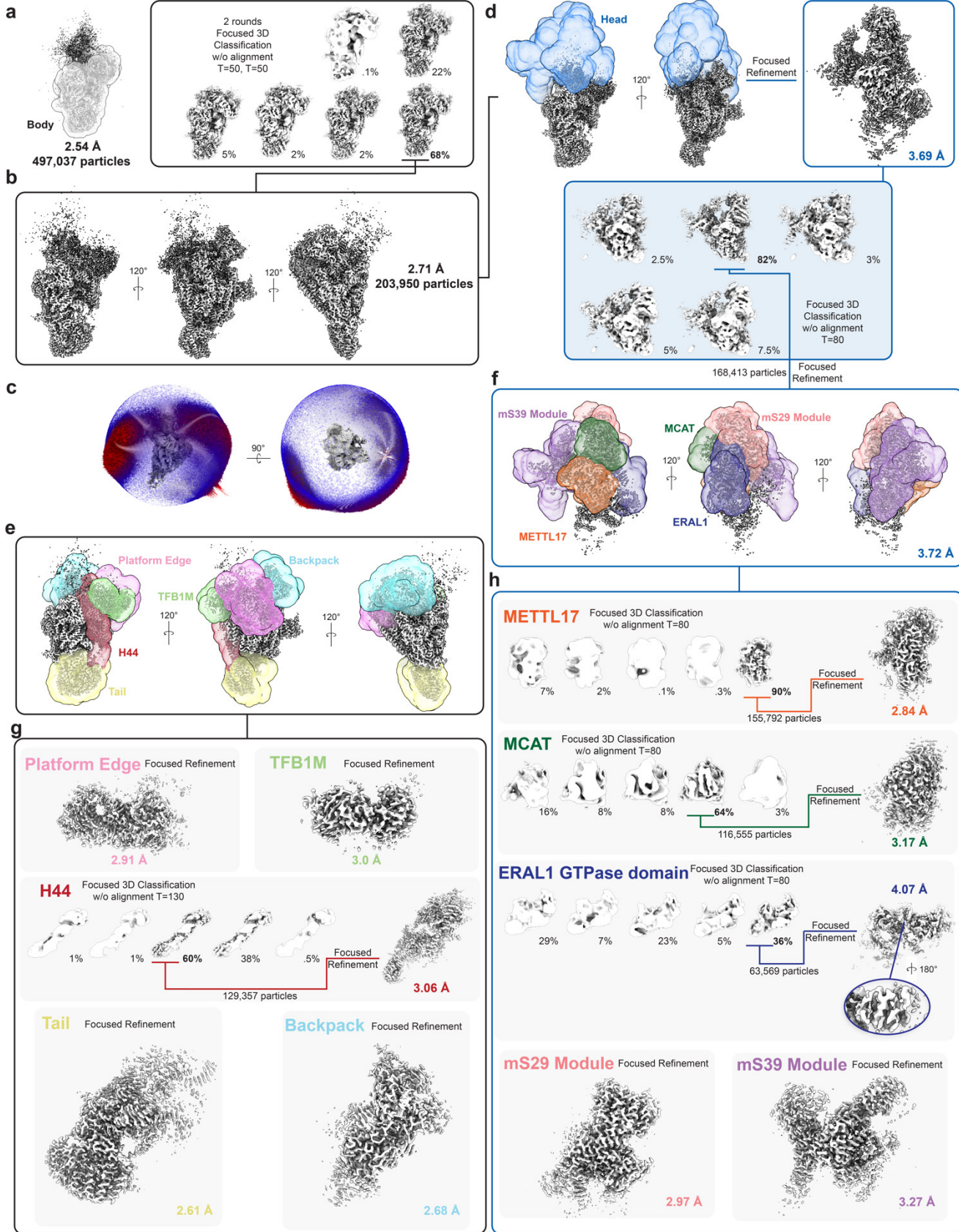
## State A



**Supplementary Fig. 4. Cryo-EM processing of human State A.**

(a) Different views of the State A overall map. (b) Euler angle distribution of the overall refinement. (c) Focused refinement and classification of the head domain. (d) Masks used in focused classification and refinement for modules in the body domain. (e) Masks used in focused classification and refinement for modules in the head domain. (f,g) Workflows for focused 3D classification and refinements. Reported resolutions (FSC=0.143) from Relion post-processing are reported next to individual focused maps. Masks used are color coded as in panels d and e.

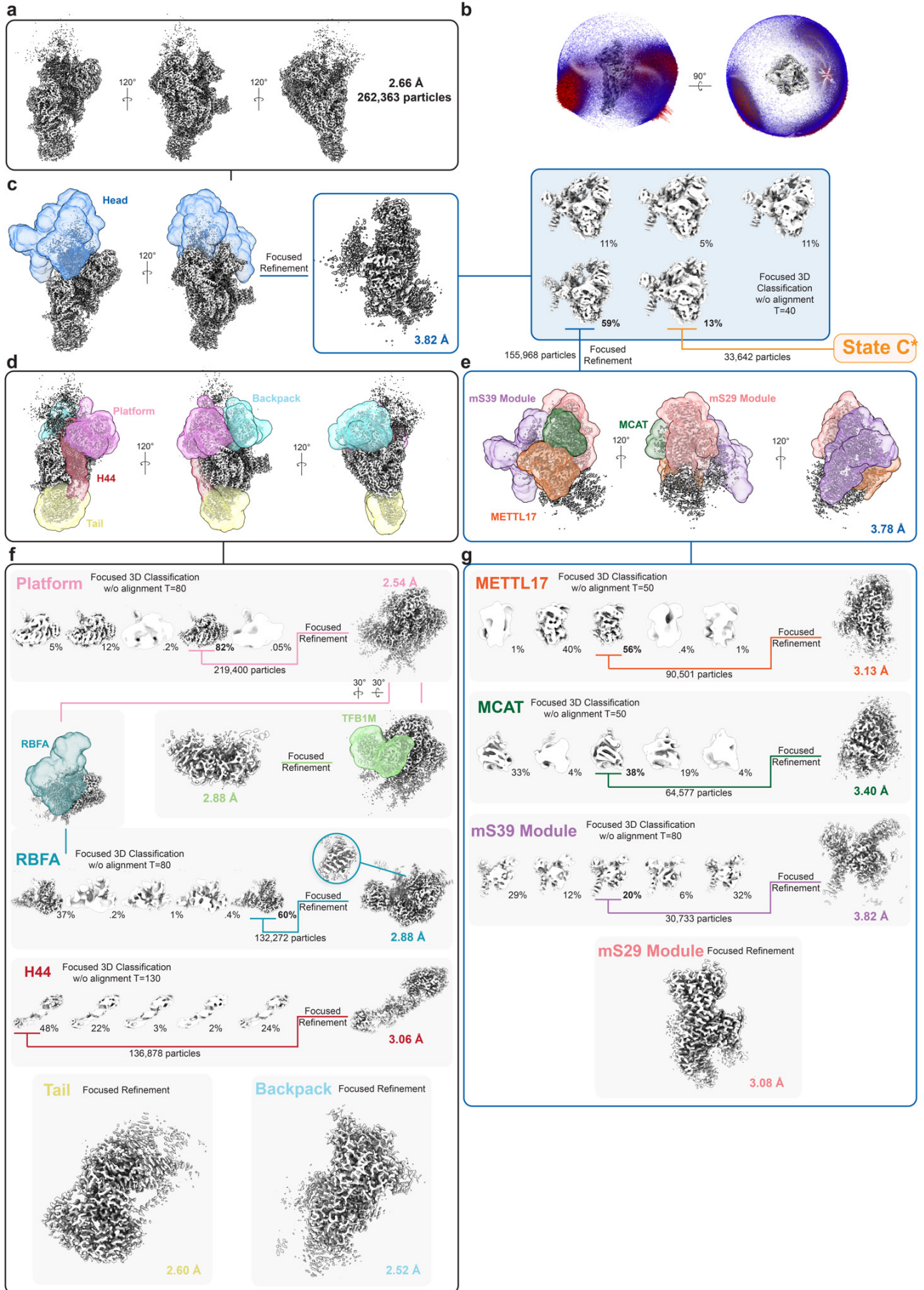
**State B**



**Supplementary Fig. 5. Cryo-EM processing of human State B.**

(a) Initial classification of particles with a body mask to clean the particle stack. (b) Different views of the State B overall map. (c) Euler angle distribution of the overall refinement. (d) Focused refinement and classification of the head domain. (e) Masks used in focused classification and refinement for modules in the body domain. (f) Masks used in focused classification and refinement for modules in the head domain. (g,h) Workflows for focused 3D classification and refinements. Reported resolutions (FSC=0.143) from Relion post-processing are reported next to individual focused maps. Masks used are color coded as in panels e and f.

## State C

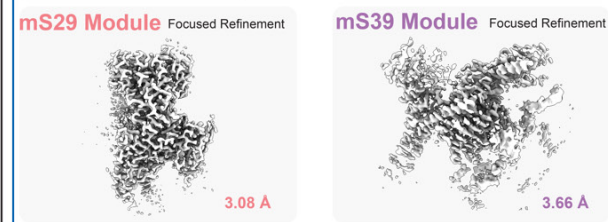
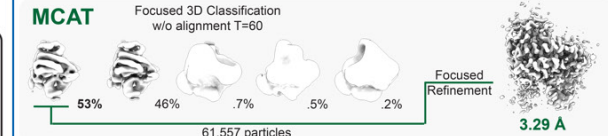
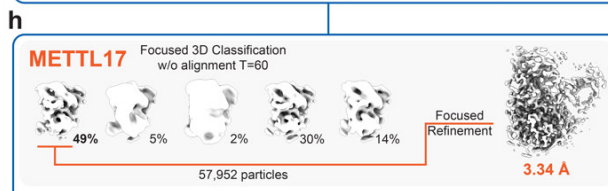
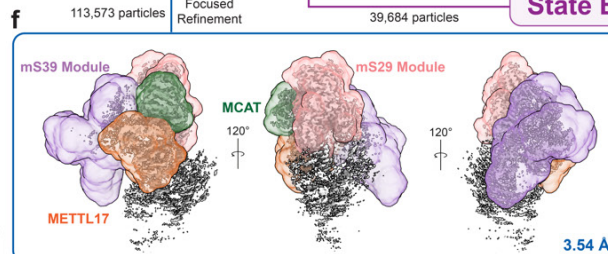
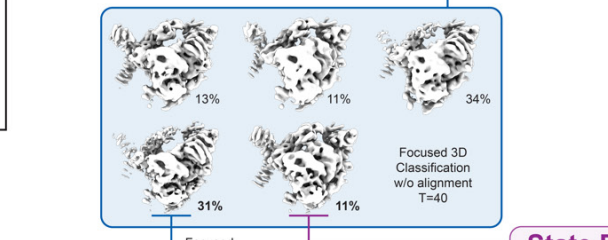
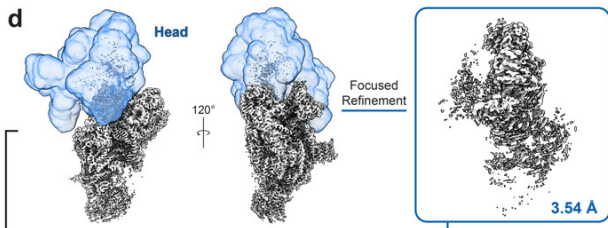
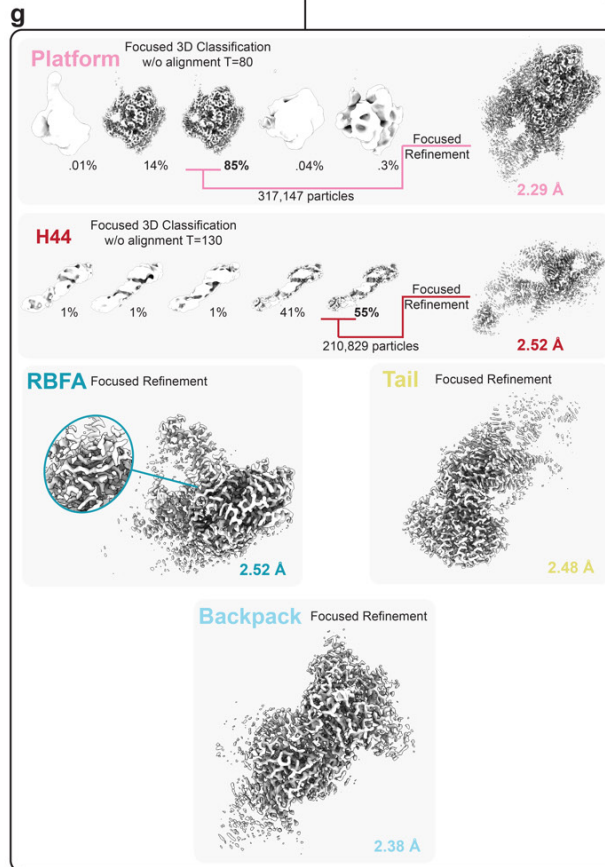
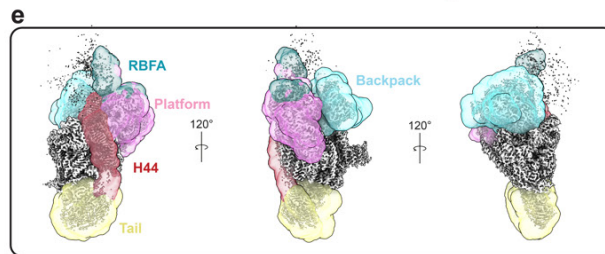
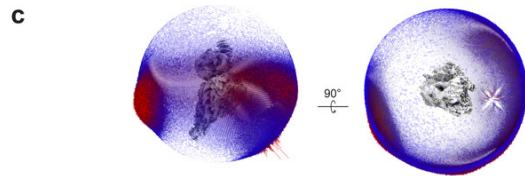
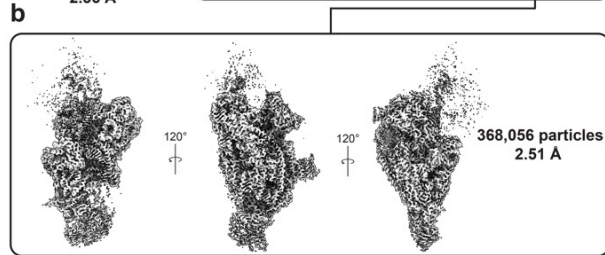
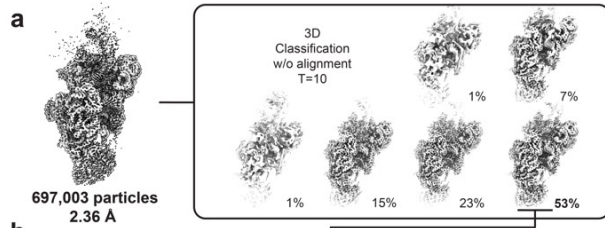


**Supplementary Fig. 6. Cryo-EM processing of human State C.**

(a) Different views of the State C overall map. (b) Euler angle distribution of the overall refinement. (c) Focused refinement and classification of the head domain. Particles identified as State C\* were further processed independently (Supplementary Fig. 9). (d) Masks used in focused classification and refinement for modules in the body domain. (e) Masks used in focused classification and refinement for modules in the head domain. (f,g) Workflows for focused 3D classification and refinements. Reported resolutions (FSC=0.143) from Relion post-processing are reported next to individual focused maps. Masks used are color coded as in panels d and e.



**State D**

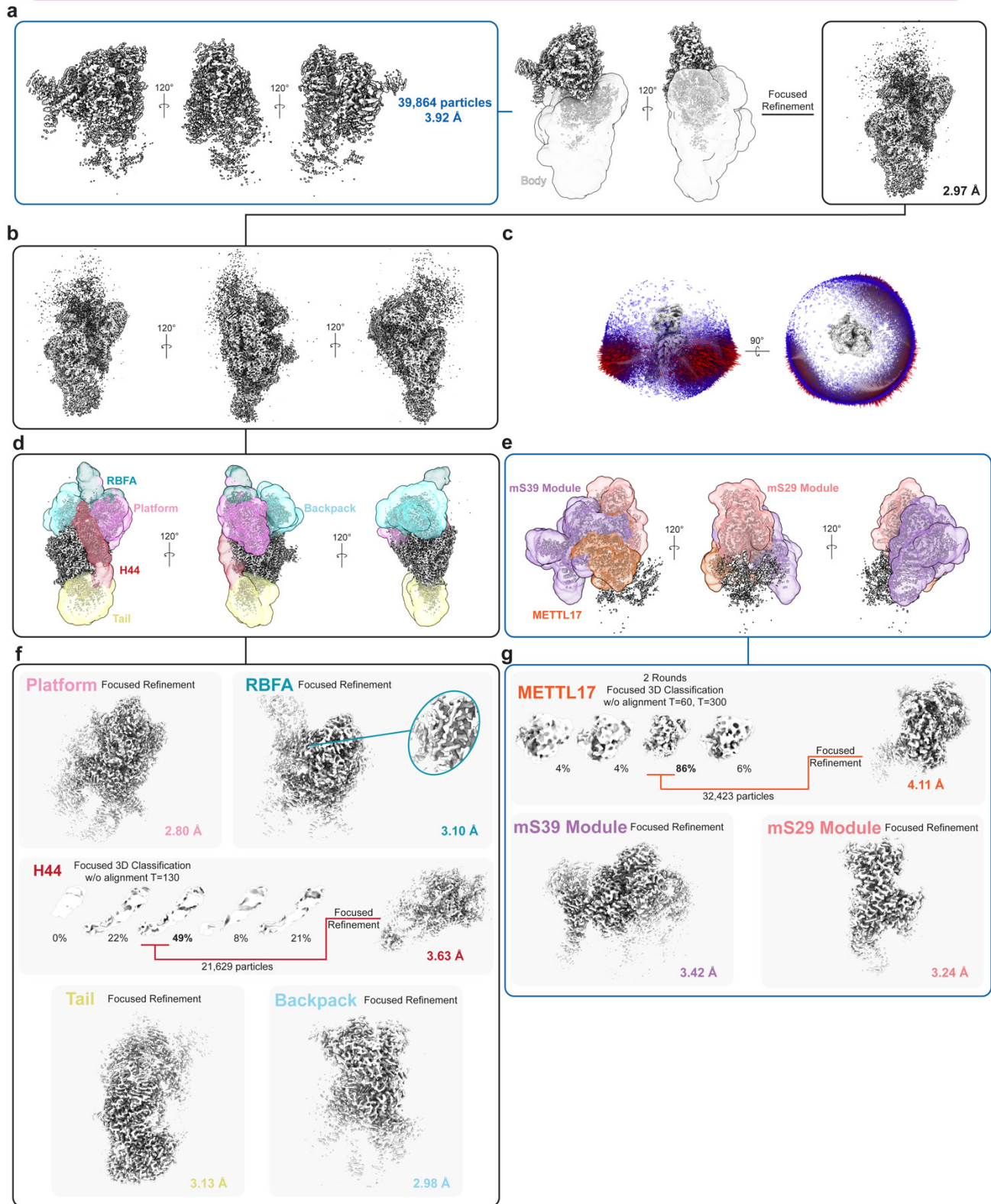


**State E**

### **Supplementary Fig. 7. Cryo-EM processing of human State D.**

(a) Initial classification of particles without a mask to clean the particle stack. (b) Different views of the State D overall map. (c) Euler angle distribution of the overall refinement. (d) Focused refinement and classification of the head domain. Particles identified as State E were further processed independently (Supplementary Fig. 8). (e) Masks used in focused classification and refinement for modules in the body domain. (f) Masks used in focused classification and refinement for modules in the head domain. (g,h) Workflows for focused 3D classification and refinements. Reported resolutions (FSC=0.143) from Relion post-processing are reported next to individual focused maps. Masks used are color coded as in panels e and f.

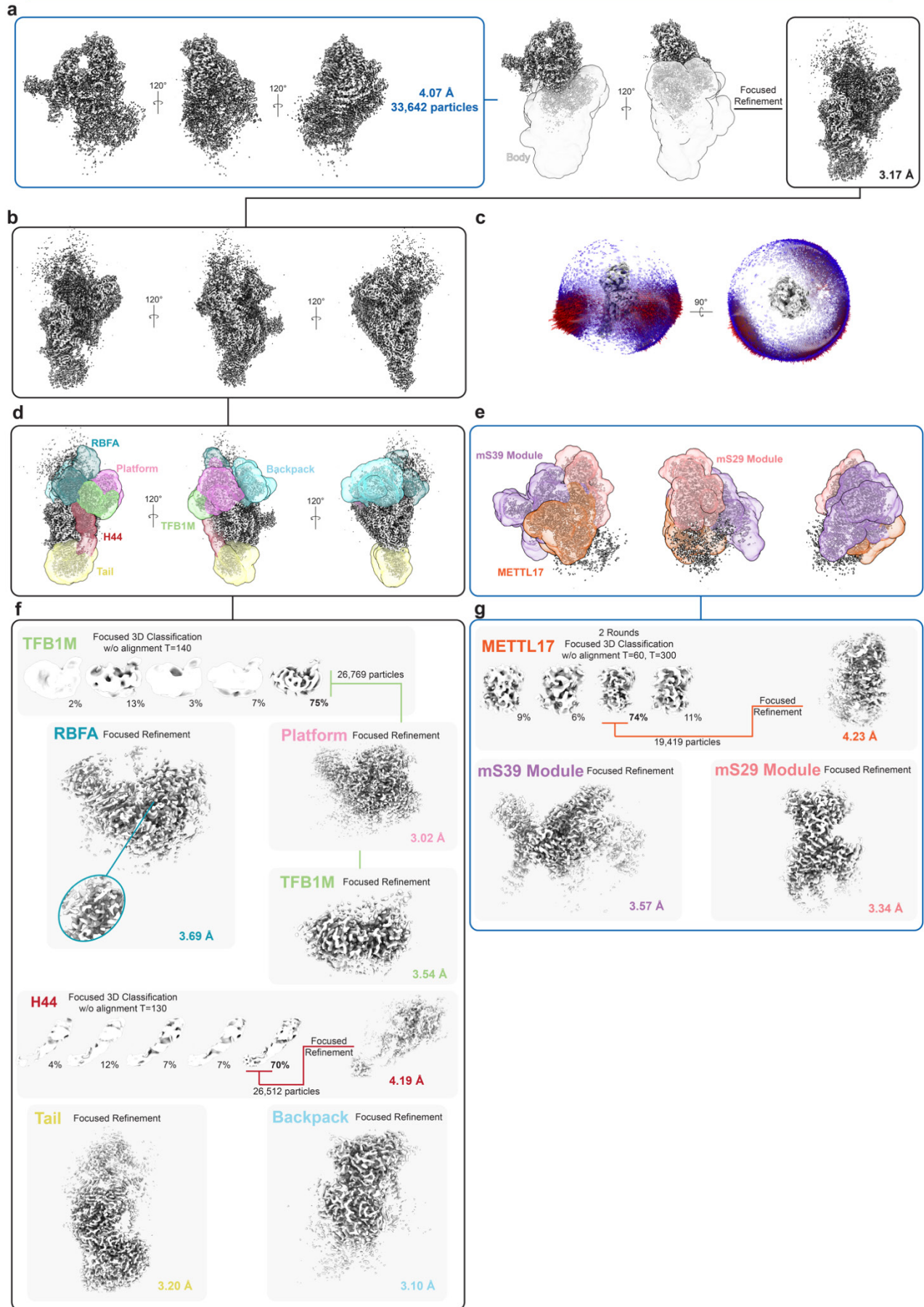
**State E**



**Supplementary Fig. 8. Cryo-EM processing of human State E.**

(a) Different views of the State E head map. Particles were then refined using a mask on the body. (b) Different views of the body domain. (c) Euler angle distribution of the overall (body) refinement. (d) Masks used in focused classification and refinement for modules in the body domain. (e) Masks used in focused classification and refinement for modules in the head domain. (f,g) Workflows for focused 3D classification and refinements. Reported resolutions (FSC=0.143) from Relion post-processing are reported next to individual focused maps. Masks used are color coded as in panels d and e.

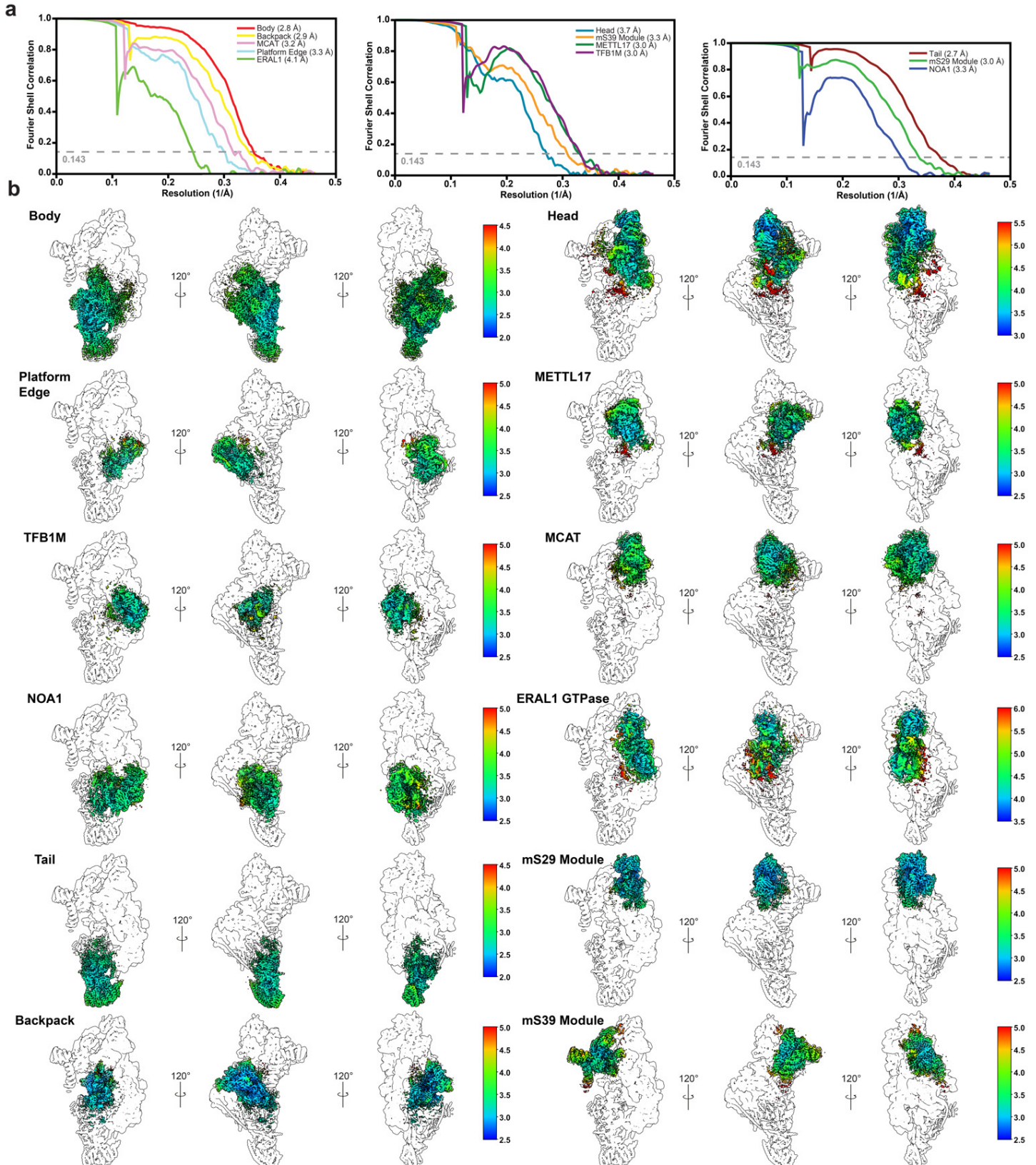
State C\*



**Supplementary Fig. 9. Cryo-EM processing of human State C\*.**

(a) Different views of the State C\* head map. Particles were then refined using a mask on the body. (b) Different views of the body domain. (c) Euler angle distribution of the overall (body) refinement. (d) Masks used in focused classification and refinement for modules in the body domain. (e) Masks used in focused classification and refinement for modules in the head domain. (f,g) Workflows for focused 3D classification and refinements. Reported resolutions (FSC=0.143) from Relion post-processing are reported next to individual focused maps. Masks used are color coded as in panels d and e.

## State A

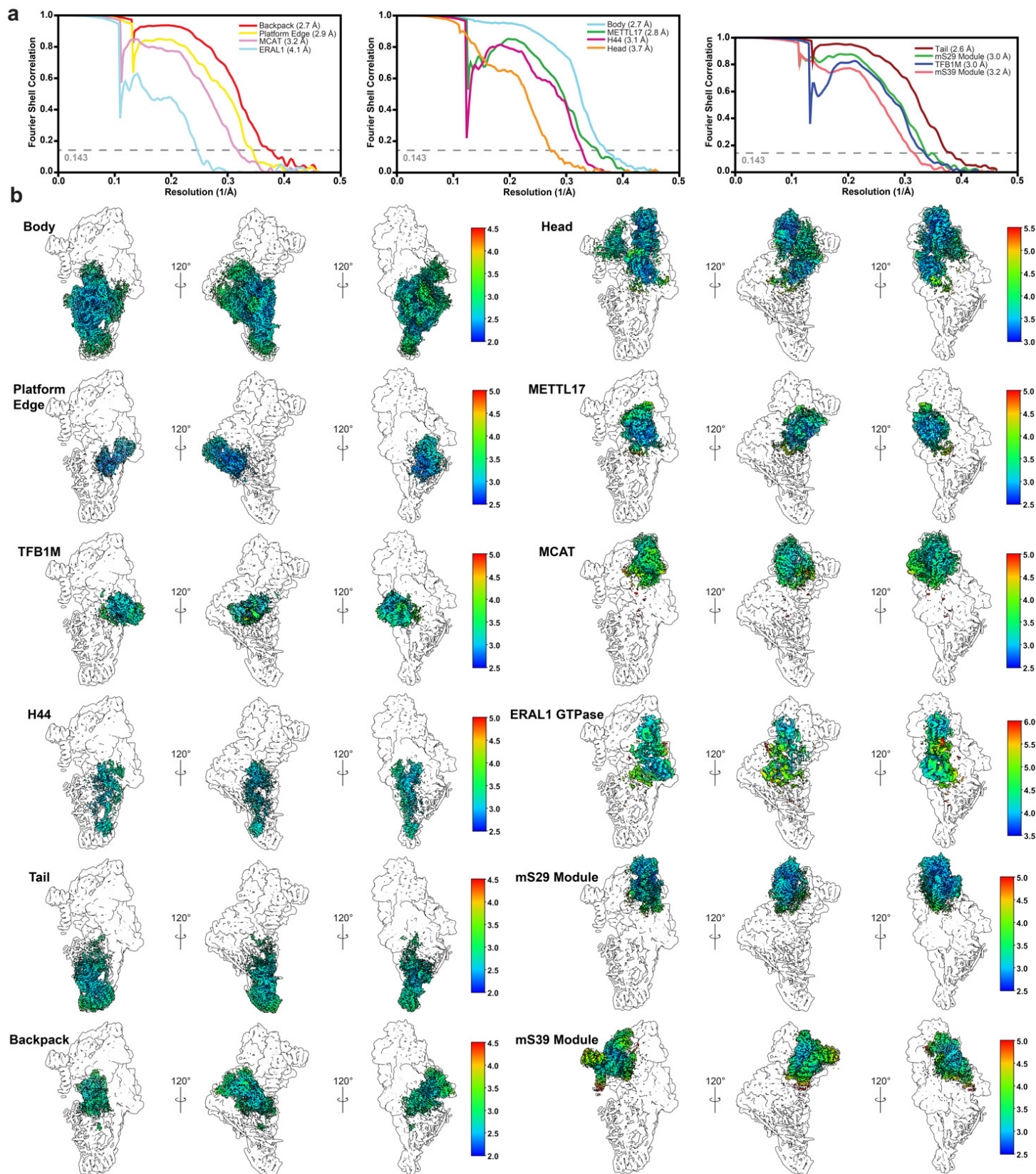


**Supplementary Fig. 10. Local resolution analysis of human State A.**

(a) Solvent-corrected FSC curves for each focused refinement determined at FSC=0.143 via post-processing in Relion. (b) Local resolution estimation (calculated in Relion) for each focused map in context with the rest of the reconstruction.



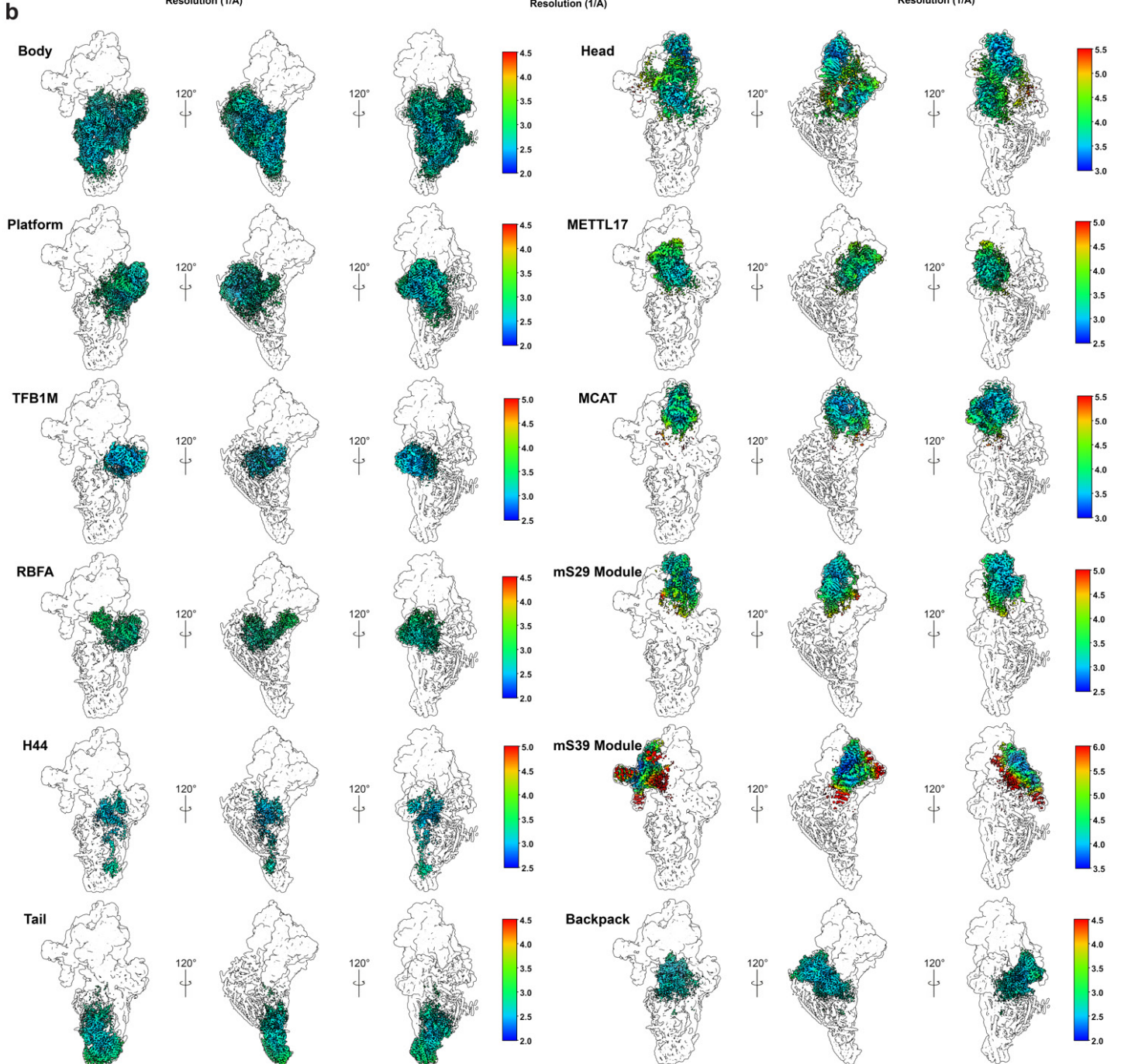
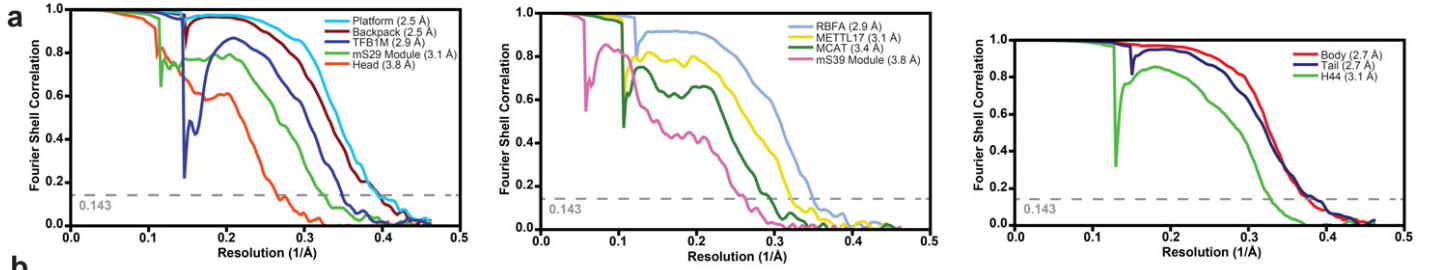
## State B



**Supplementary Fig. 11. Local resolution analysis of human State B.**

(a) Solvent-corrected FSC curves for each focused refinement determined at FSC=0.143 via post-processing in Relion. (b) Local resolution estimation (calculated in Relion) for each focused map in context with the rest of the reconstruction.

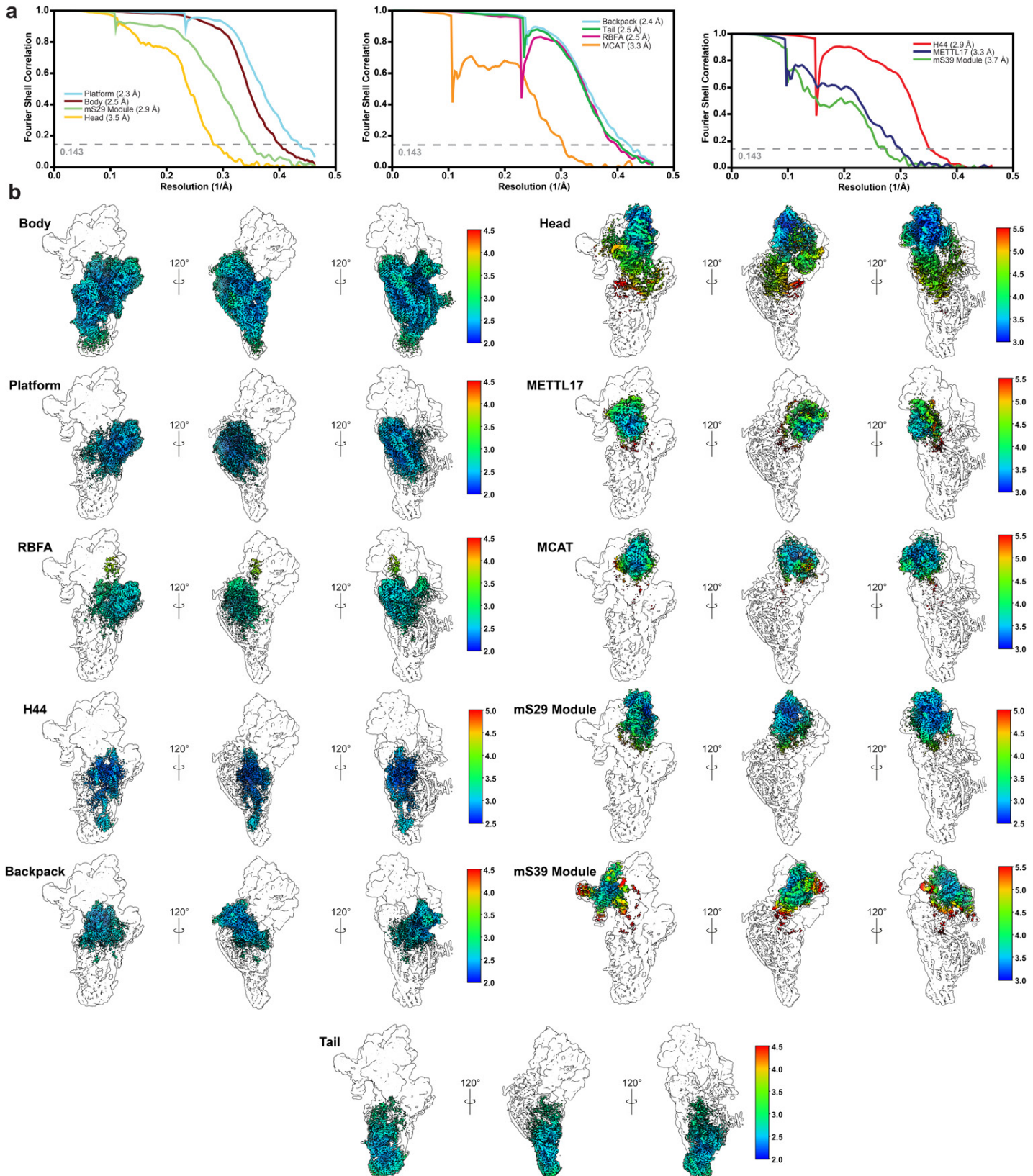
## State C



**Supplementary Fig. 12. Local resolution analysis of human State C.**

(a) Solvent-corrected FSC curves for each focused refinement determined at FSC=0.143 via post-processing in Relion. (b) Local resolution estimation (calculated in Relion) for each focused map in context with the rest of the reconstruction.

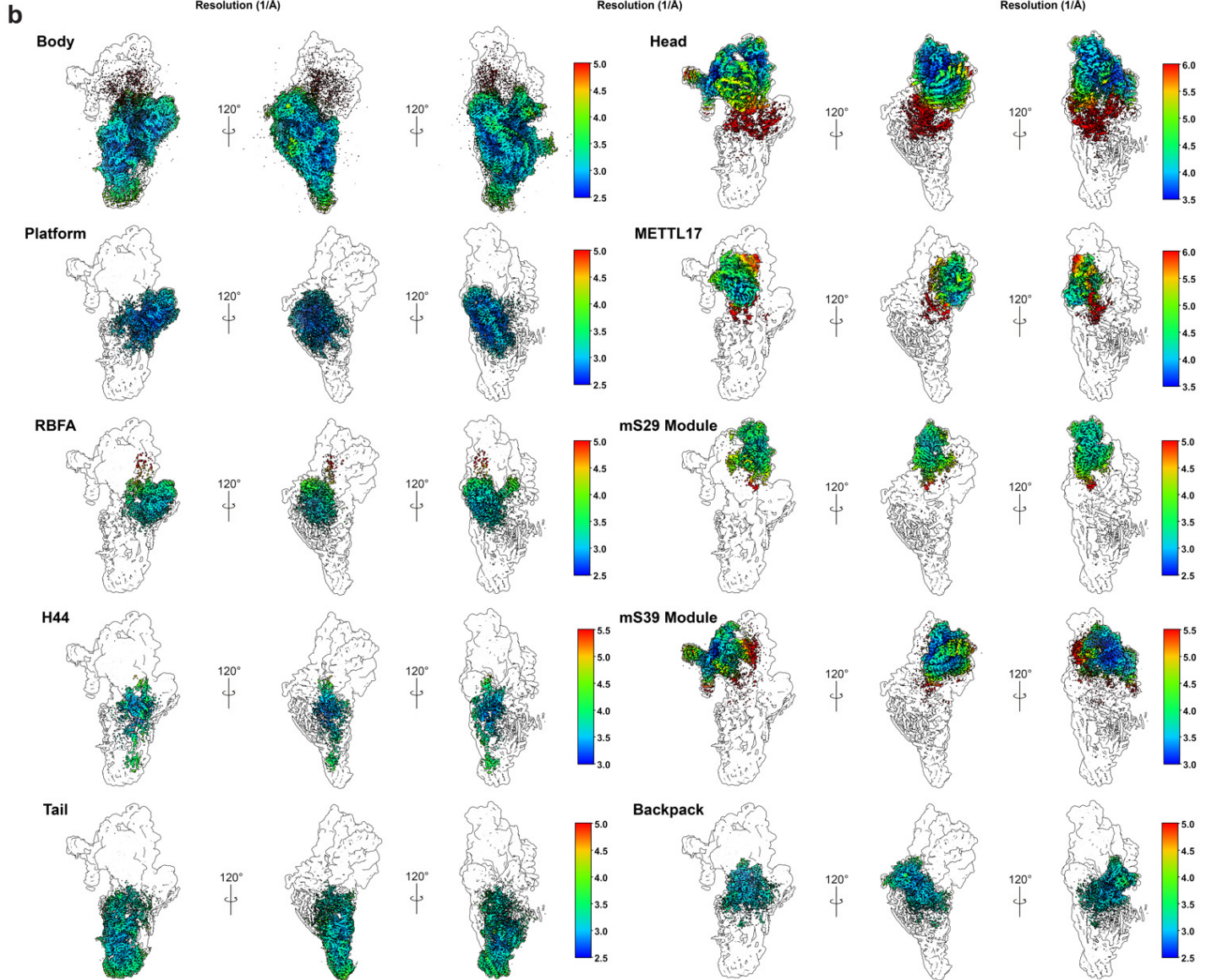
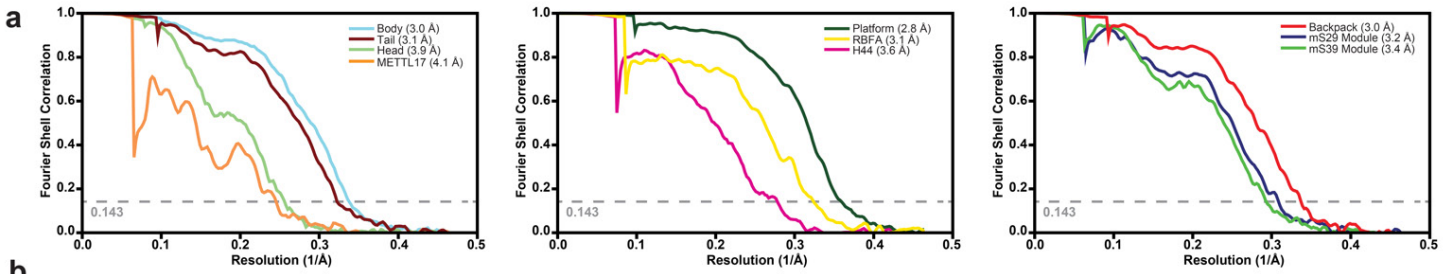
## State D



**Supplementary Fig. 13. Local resolution analysis of human State D.**

(a) Solvent-corrected FSC curves for each focused refinement determined at FSC=0.143 via post-processing in Relion. (b) Local resolution estimation (calculated in Relion) for each focused map in context with the rest of the reconstruction.

## State E

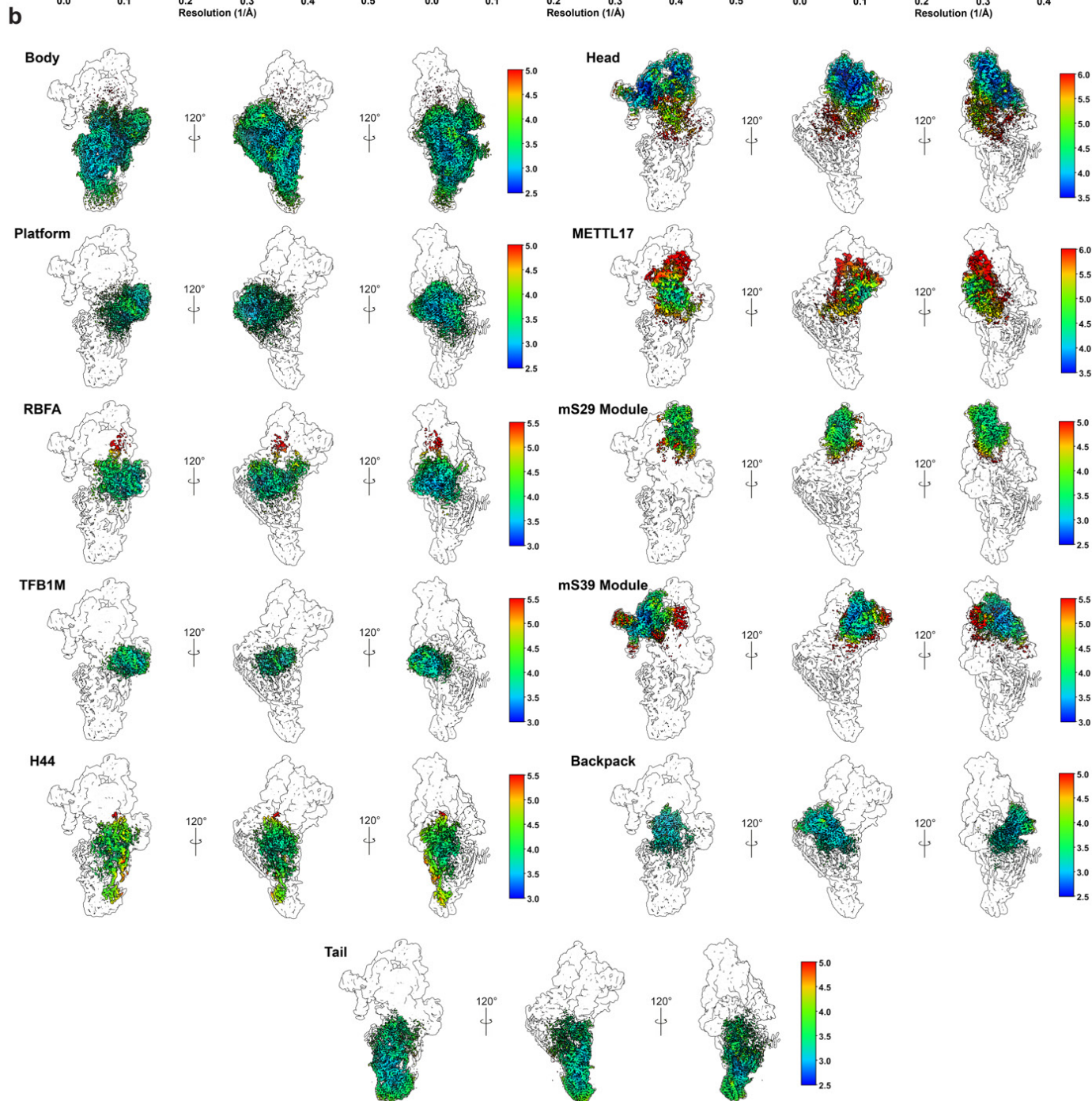
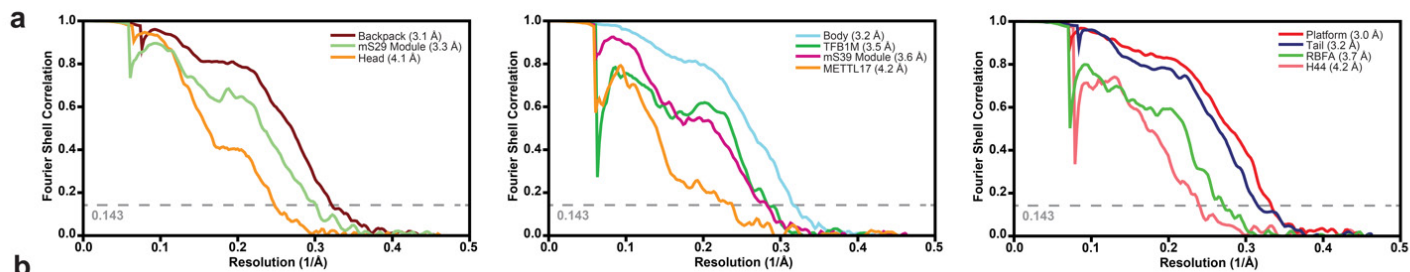


**Supplementary Fig. 14. Local resolution analysis of human State E.**

(a) Solvent-corrected FSC curves for each focused refinement determined at FSC=0.143 via post-processing in Relion. (b) Local resolution estimation (calculated in Relion) for each focused map in context with the rest of the reconstruction.



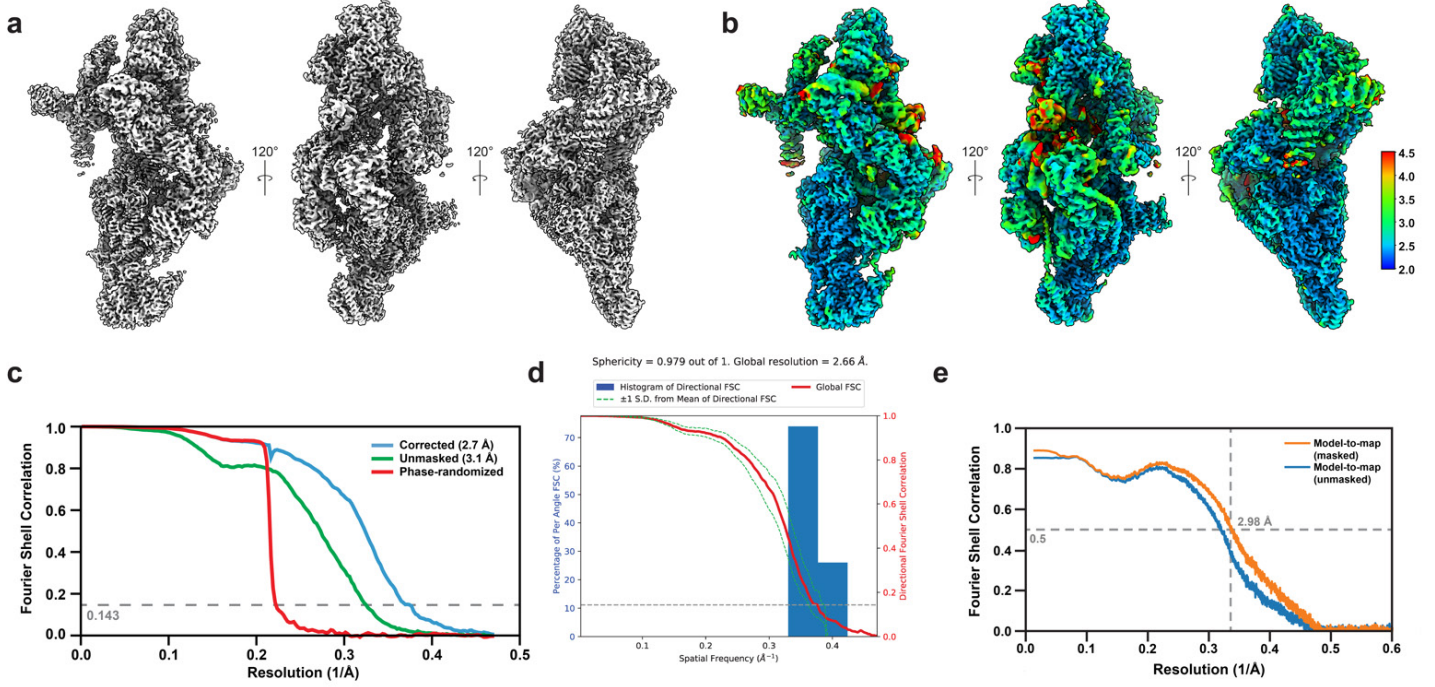
## State C\*



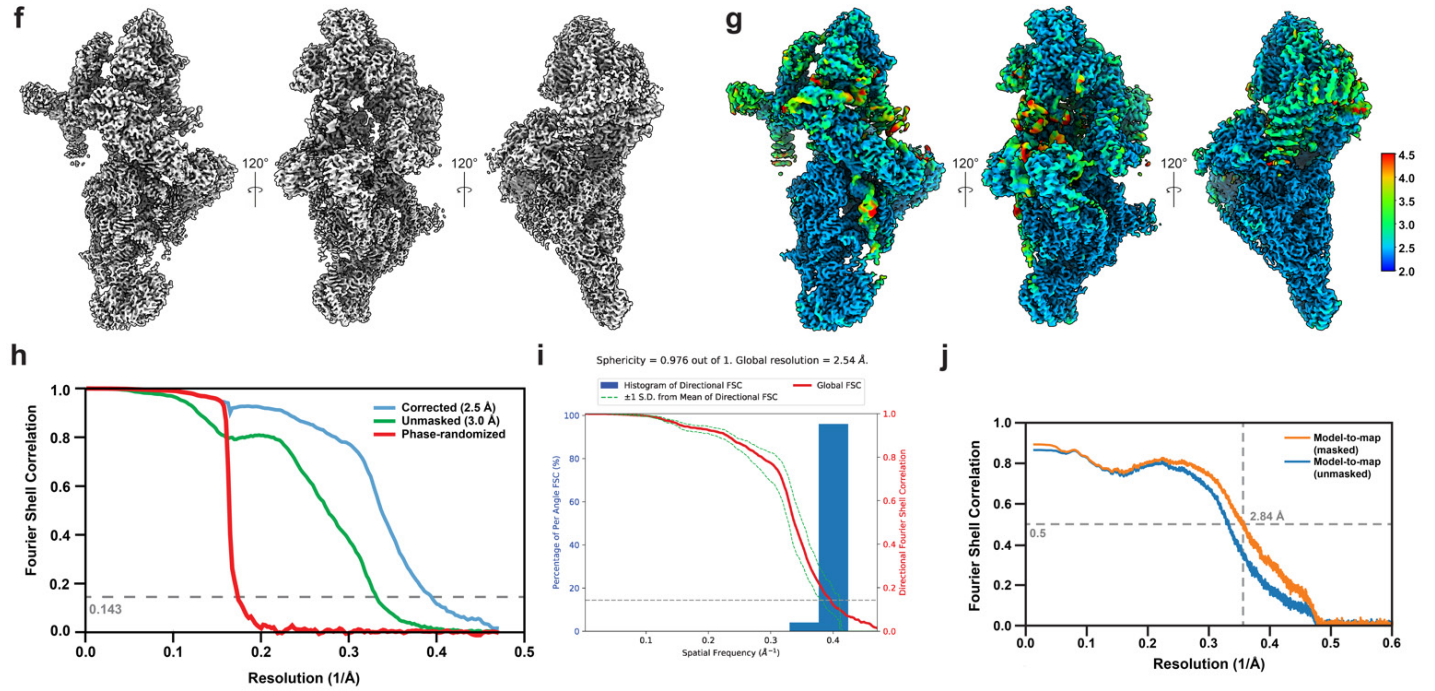
**Supplementary Fig. 15. Local resolution analysis of human State C\*.**

(a) Solvent-corrected FSC curves for each focused refinement determined at FSC=0.143 via post-processing in Relion. (b) Local resolution estimation (calculated in Relion) for each focused map in context with the rest of the reconstruction.

## State A



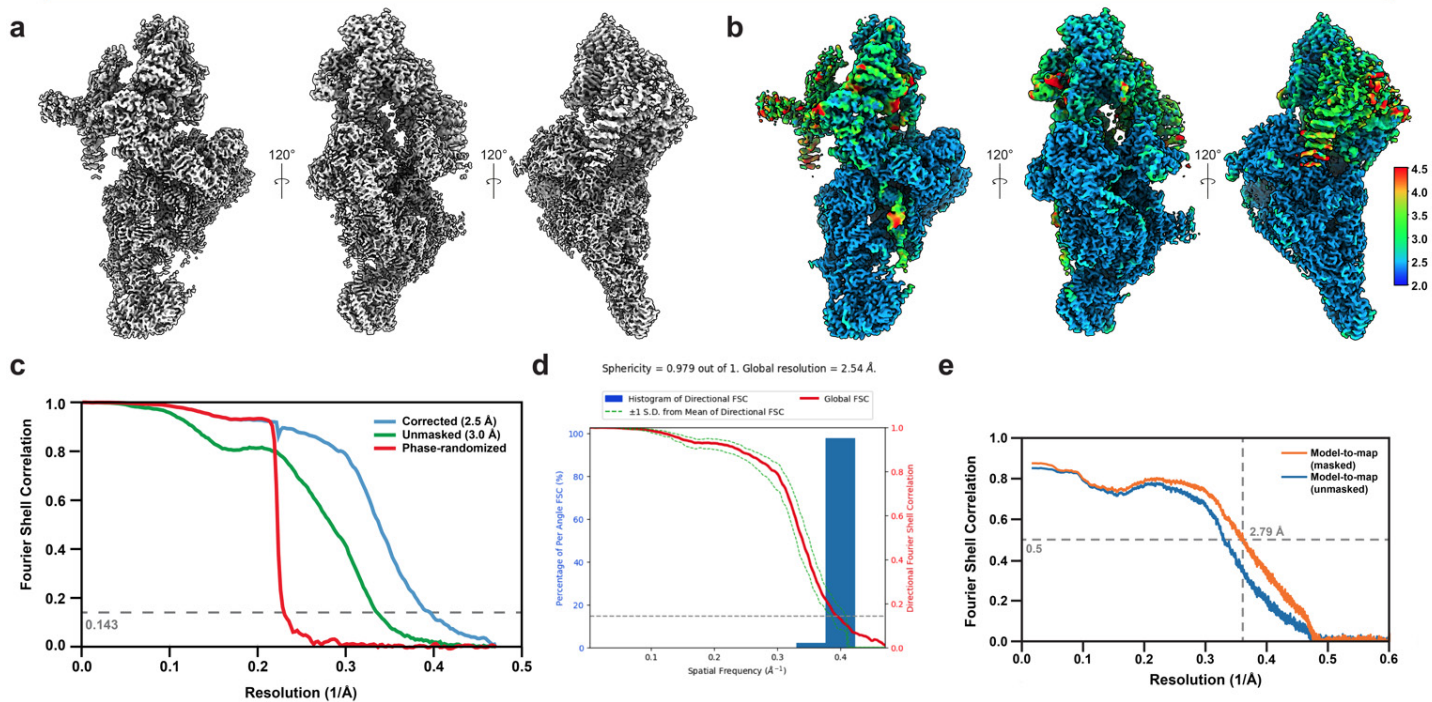
## State B



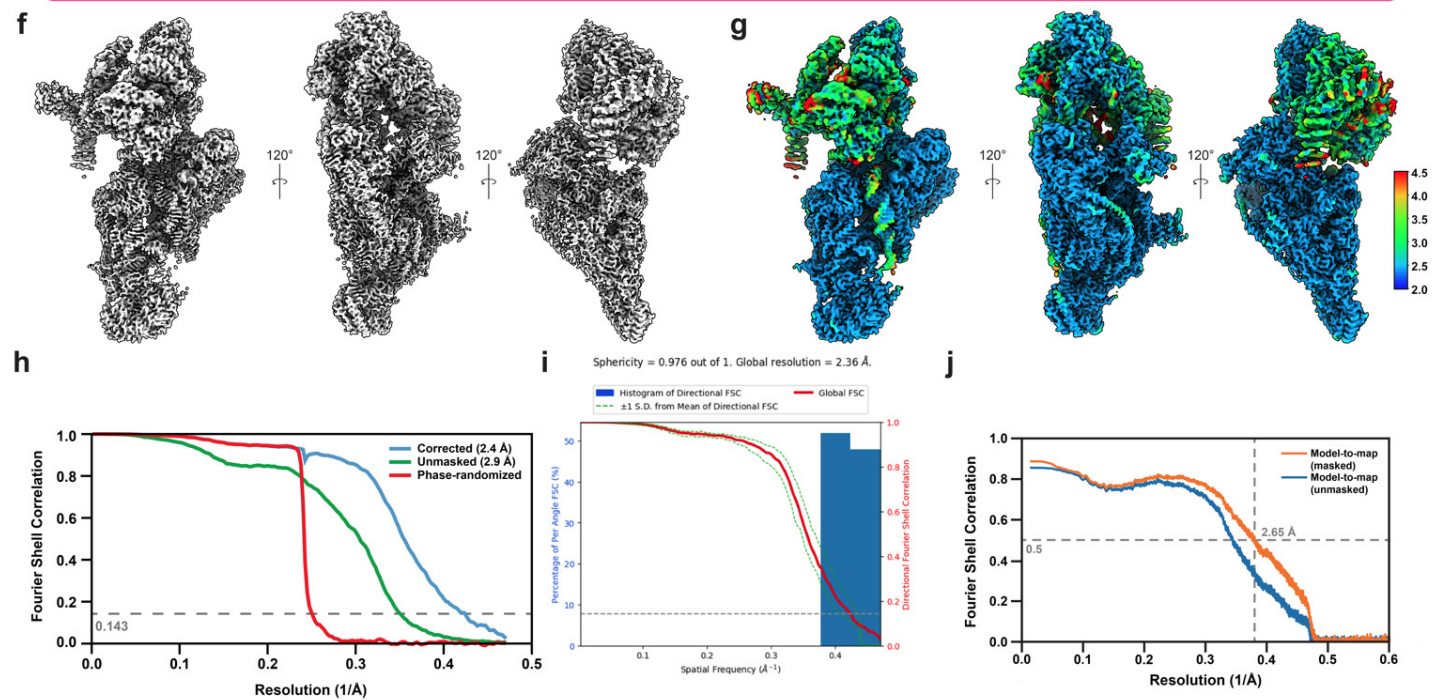
**Supplementary Fig. 16. Validation of composite maps for human States A and B.**

(a) Different views of the composite map of State A. (b) Different views of the composite map of State A filtered and colored according to local resolution as calculated by cryoSPARC. (c) FSC curves for the State A composite map as calculated in Relion. Reported resolutions were determined at FSC=0.143. (d) 3DFSC for the State A composite map calculated using the Remote 3DFSC Processing Server<sup>1</sup>. (e) Map-to-model correlation between the State A composite map and the State A model. (f) Different views of the composite map of State B. (g) Different views of the composite map of State B filtered and colored according to local resolution as calculated by cryoSPARC. (h) FSC curves for the State B composite map as calculated in Relion. Reported resolutions were determined at FSC=0.143. (i) 3DFSC for the State B composite map calculated using the Remote 3DFSC Processing Server<sup>1</sup>. (j) Map-to-model correlation between the State B composite map and the State B model.

## State C



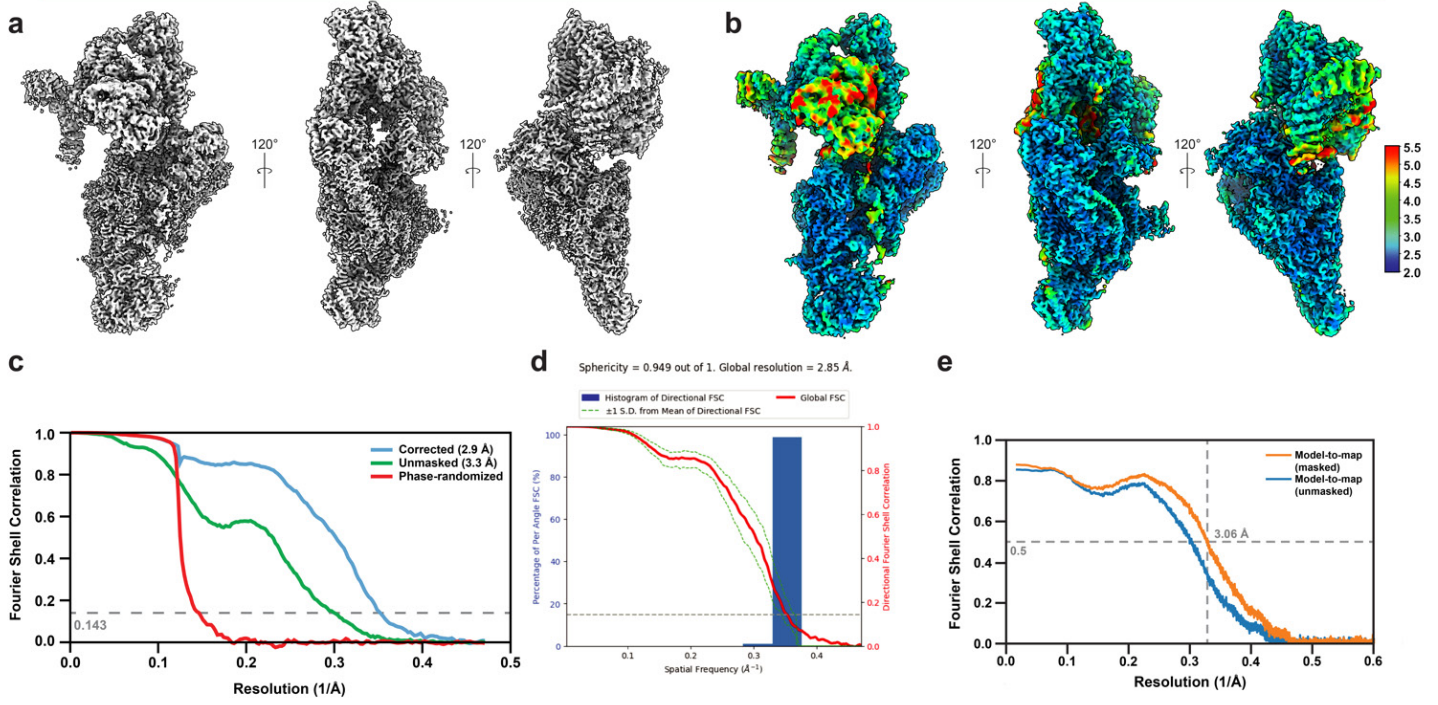
## State D



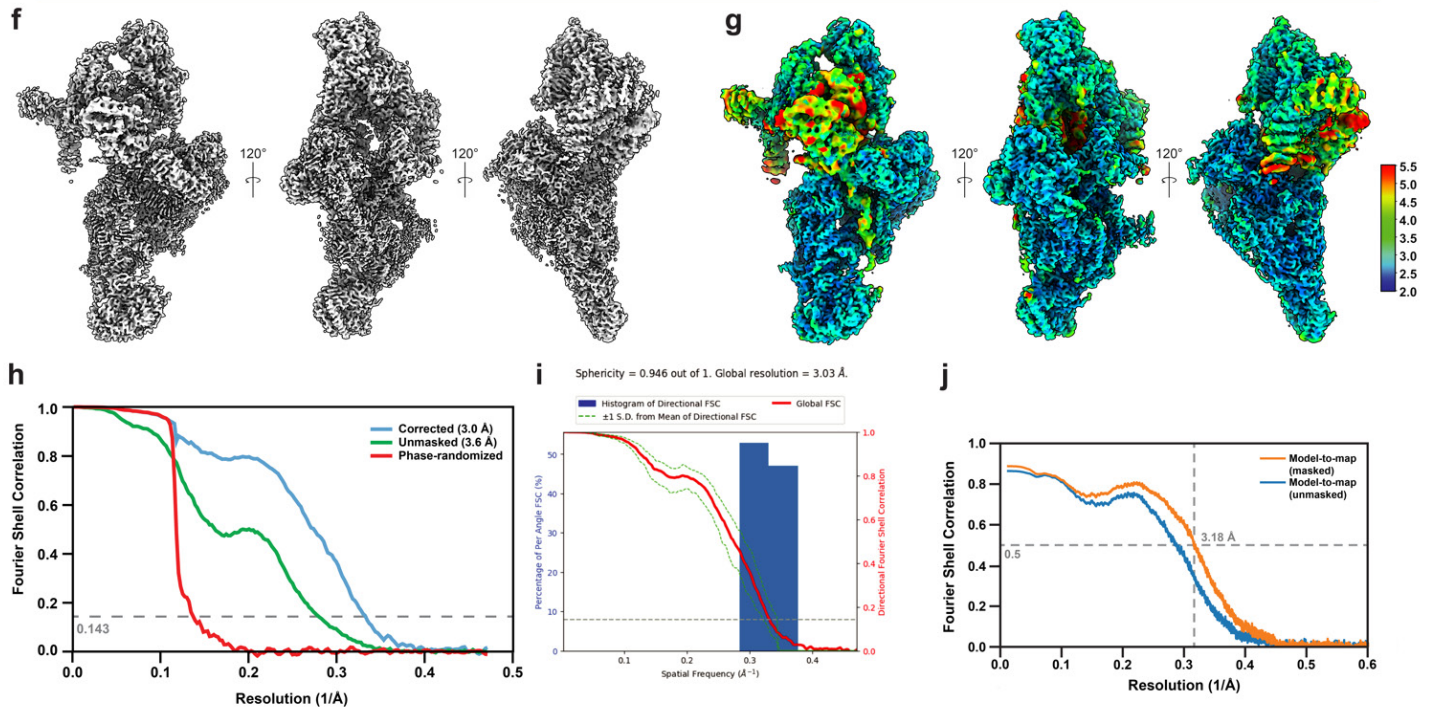
**Supplementary Fig. 17. Validation of composite maps for human States C and D.**

(a) Different views of the composite map of State C. (b) Different views of the composite map of State C filtered and colored according to local resolution as calculated by cryoSPARC. (c) FSC curves for the State C composite map as calculated in Relion. Reported resolutions were determined at FSC=0.143. (d) 3DFSC for the State C composite map calculated using the Remote 3DFSC Processing Server<sup>1</sup>. (e) Map-to-model correlation between the State C composite map and the State C model. (f) Different views of the composite map of State D. (g) Different views of the composite map of State D filtered and colored according to local resolution as calculated by cryoSPARC. (h) FSC curves for the State D composite map as calculated in Relion. Reported resolutions were determined at FSC=0.143. (i) 3DFSC for the State D composite map calculated using the Remote 3DFSC Processing Server<sup>1</sup>. (j) Map-to-model correlation between the State D composite map and the State D model.

## State E



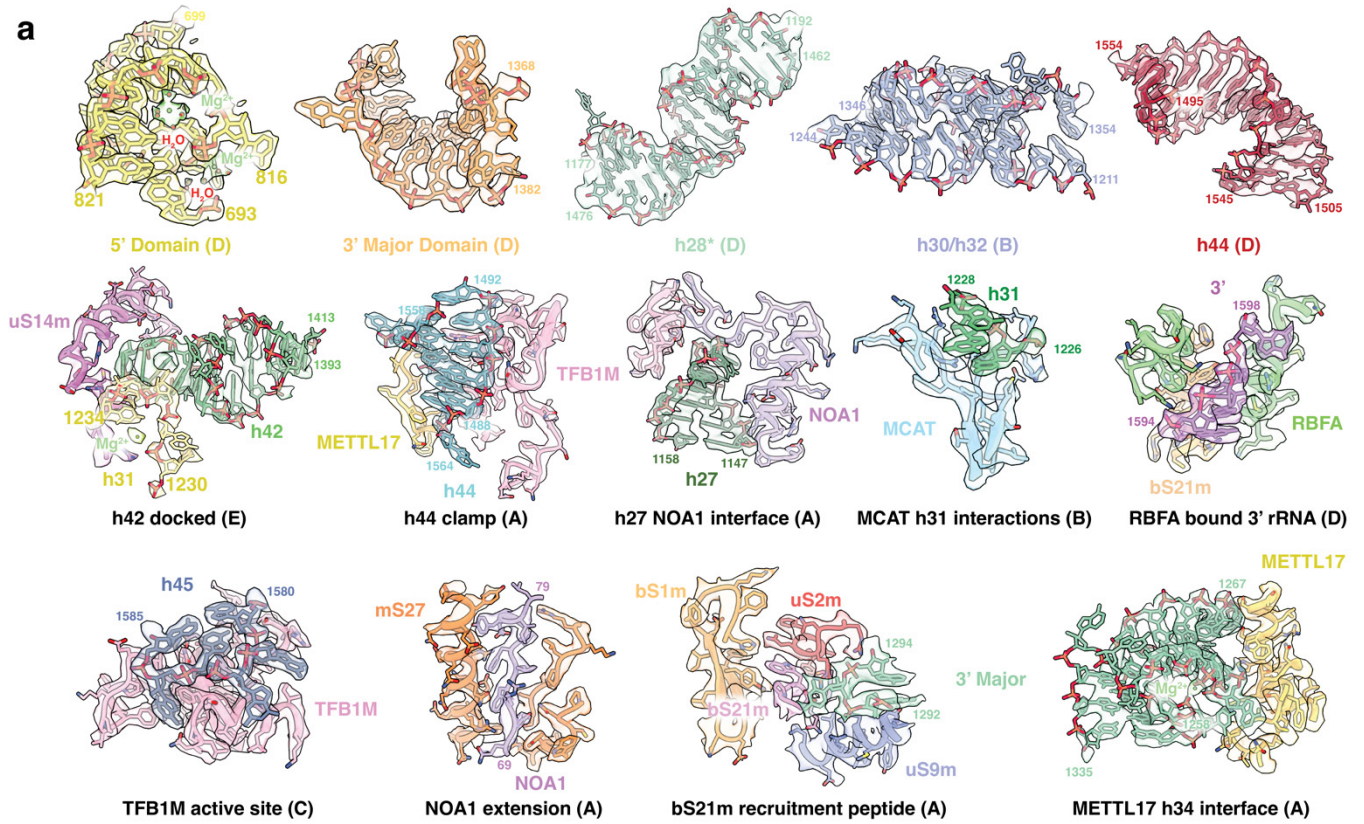
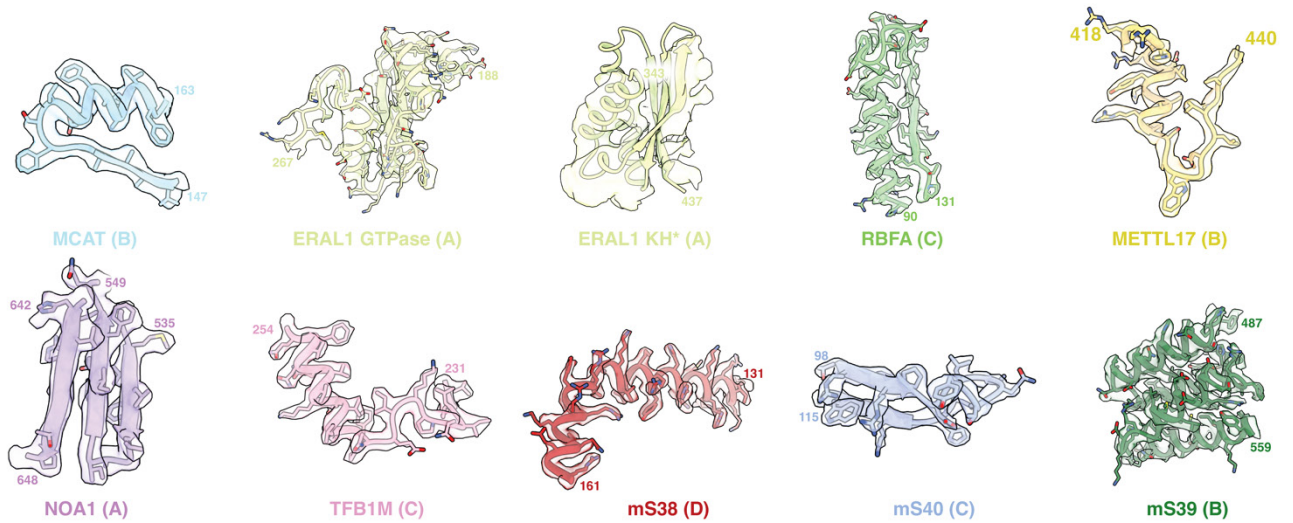
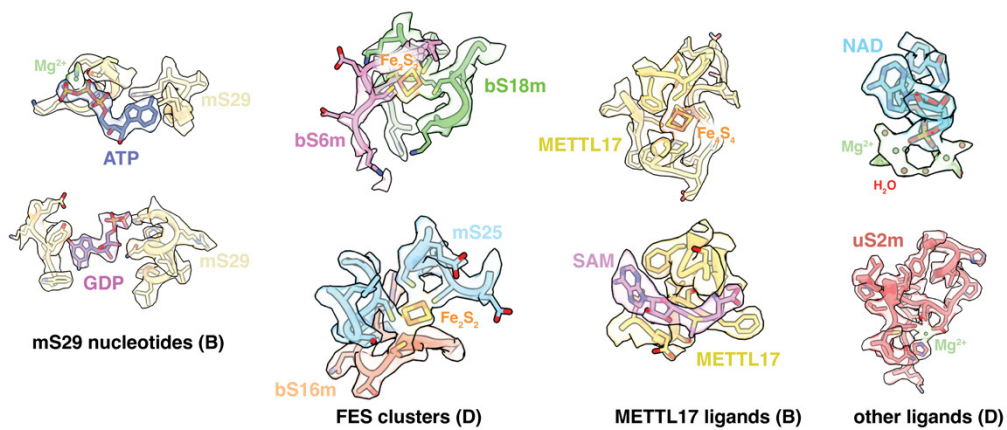
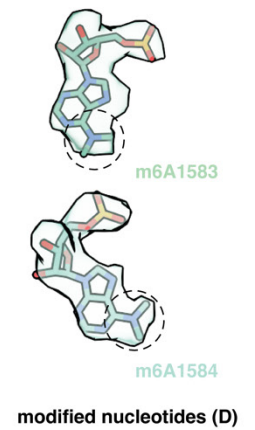
## State C\*



**Supplementary Fig. 18. Validation of composite maps for human States E and C\*.**

(a) Different views of the composite map of State E. (b) Different views of the composite map of State E filtered and colored according to local resolution as calculated by cryoSPARC. (c) FSC curves for the State E composite map as calculated in Relion. Reported resolutions were determined at FSC=0.143. (d) 3DFSC for the State E composite map calculated using the Remote 3DFSC Processing Server<sup>1</sup>. (e) Map-to-model correlation between the State E composite map and the State E model. (f) Different views of the composite map of State C\*. (g) Different views of the composite map of State C\* filtered and colored according to local resolution as calculated by cryoSPARC. (h) FSC curves for the State C\* composite map as calculated in Relion. Reported resolutions were determined at FSC=0.143. (i) 3DFSC for the State C\* composite map calculated using the Remote 3DFSC Processing Server<sup>1</sup>. (j) Map-to-model correlation between the State C\* composite map and the State C\* model.

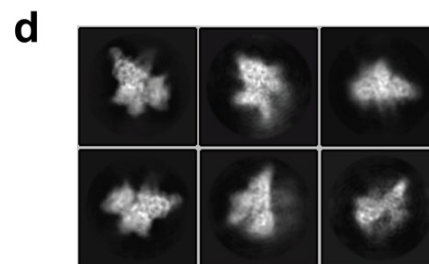
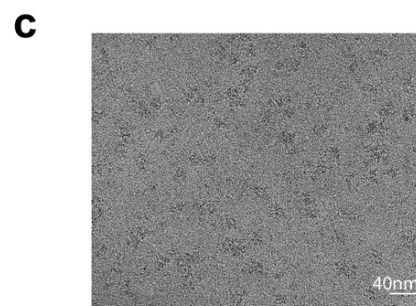
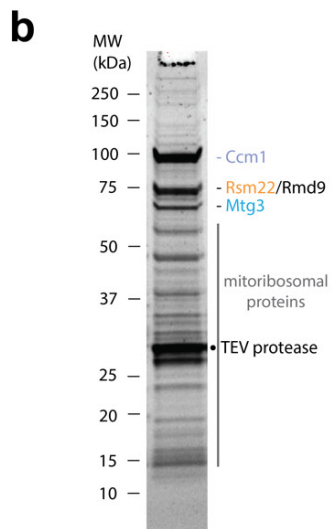
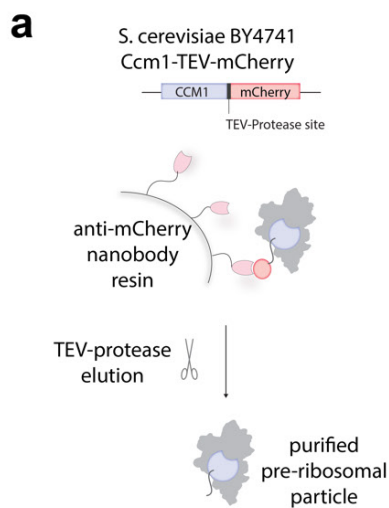


**a****b****c****d**

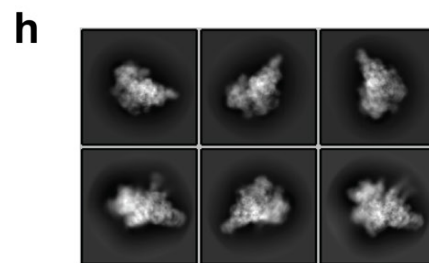
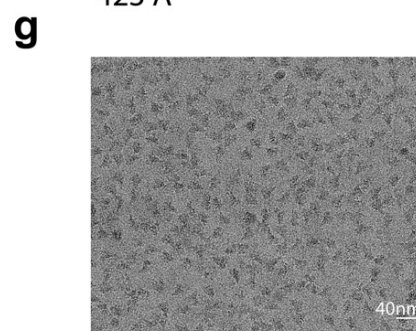
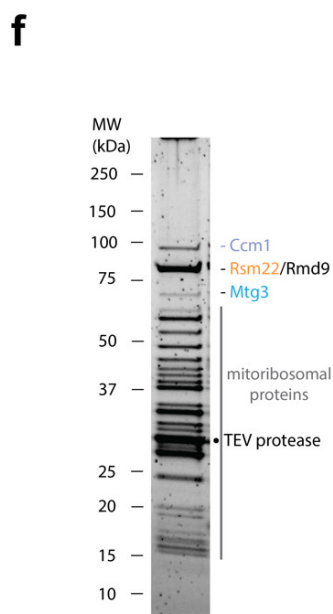
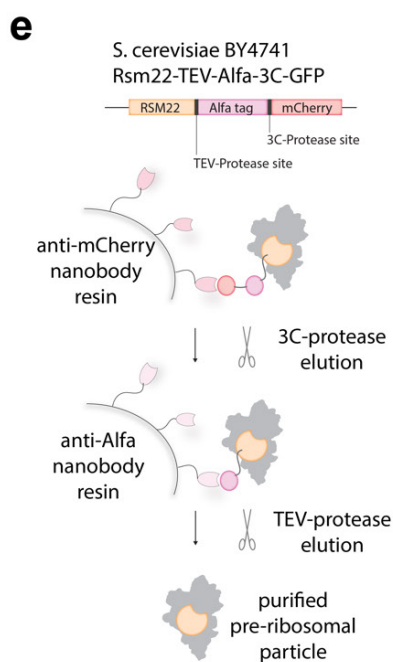
**Supplementary Fig. 19. Representative cryo-EM densities and models for human structures.**

Selections of representative densities of RNA and protein across all states, comprised of (a) rRNA and functionally relevant protein-RNA and protein-protein interfaces, (b) assembly factors and mitochondrial proteins, (c) ligands, and (d) modified nucleotides.

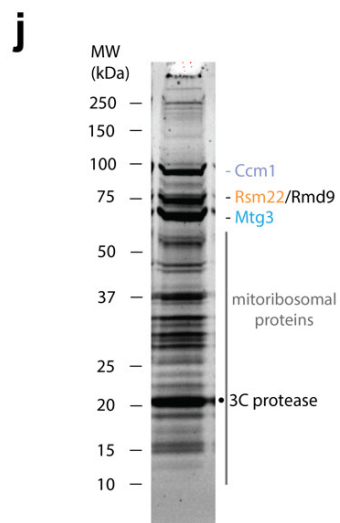
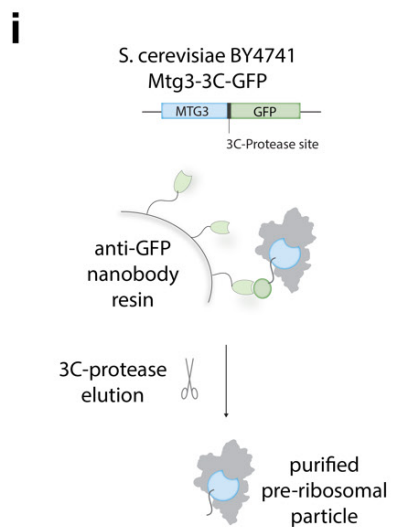
The states from which density and models are derived are shown in parentheses below each panel, and \* denotes maps that have been filtered to local resolution.



423 Å

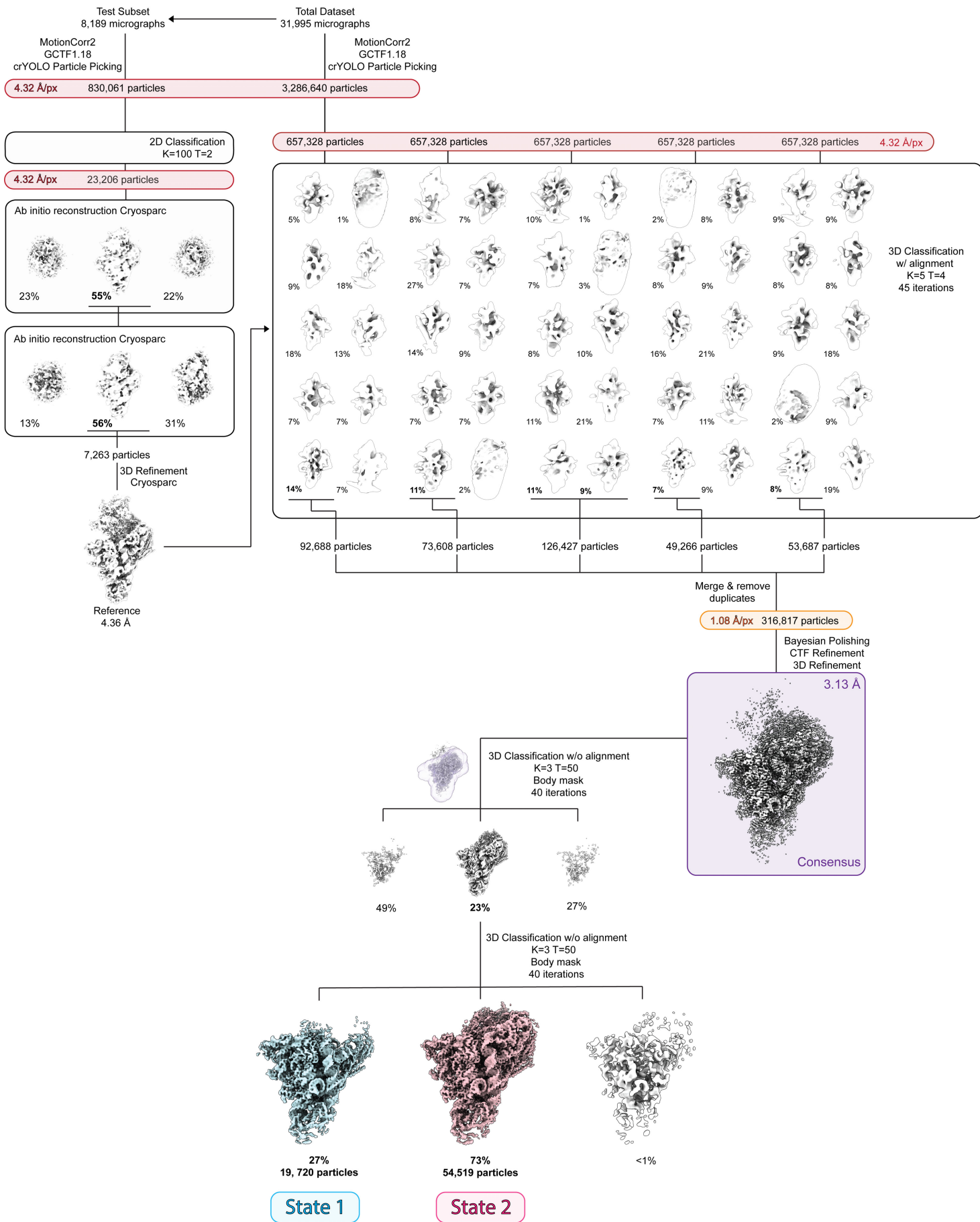


423 Å



**Supplementary Fig. 20. Purification of yeast mtSSU assembly intermediates.**

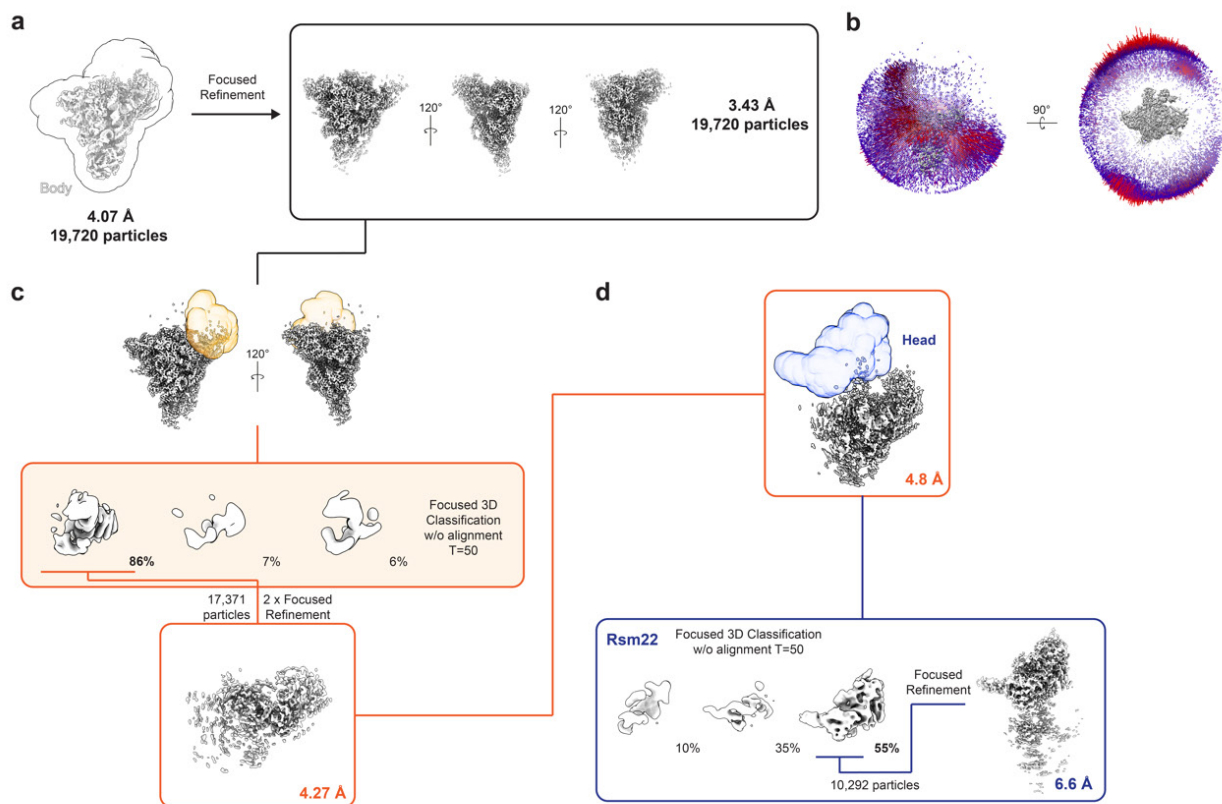
(a) Purification scheme for Ccm1-containing mitoribosomal intermediates. (b) Representative SDS-PAGE gel of eluted Ccm1 sample. Proteins were identified with LC-MS/MS (Supplementary Data S2). Immunoprecipitation experiments were repeated at least 3 times with similar results. (c) Motion corrected cryo-EM micrograph of Ccm1-bound particles representative of 31,995 total micrographs. (d) 6 representative 2D class averages for the Ccm1 dataset (4x binned, 4.32 Å/px). (e) Purification scheme for Rsm22-containing mitoribosomal intermediates. (f) Representative SDS-PAGE gel of eluted Rsm22 sample. Proteins were identified with LC-MS/MS (Supplementary Data S3). Immunoprecipitation experiments were repeated at least 3 times with similar results. (g) Motion corrected cryo-EM micrograph of Rsm22-bound particles representative of 14,111 total micrographs. (h) 6 representative 2D class averages for the Rsm22 dataset (8x binned, 8.64 Å/px). (i) Purification scheme for Mtg3-containing mitoribosomal intermediates. (j) Representative SDS-PAGE gel of eluted Mtg3 sample. Proteins were identified with LC-MS/MS (Supplementary Data S4). Immunoprecipitation experiments were repeated at least 3 times with similar results. For gel source data, see Supplementary Fig. 1.



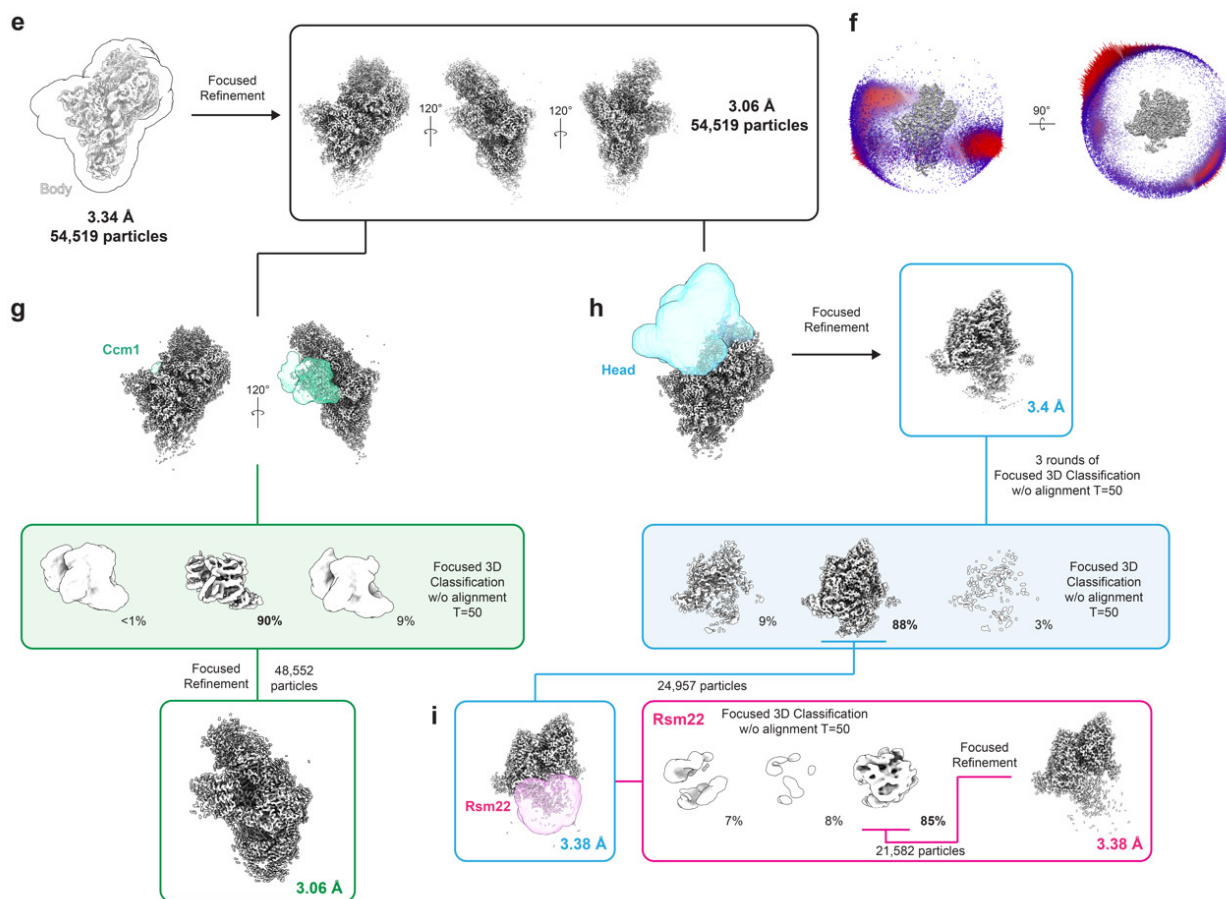
**Supplementary Fig. 21. Initial cryo-EM processing of yeast Ccm1-containing particles.**

Workflow for data processing and identification of two assembly states, States 1 and 2. Reported resolutions (FSC=0.143) from Relion post-processing are reported next to individual maps.

### State 1



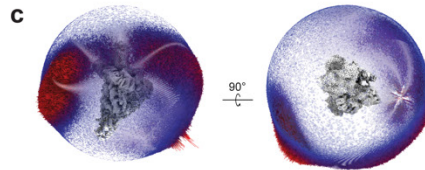
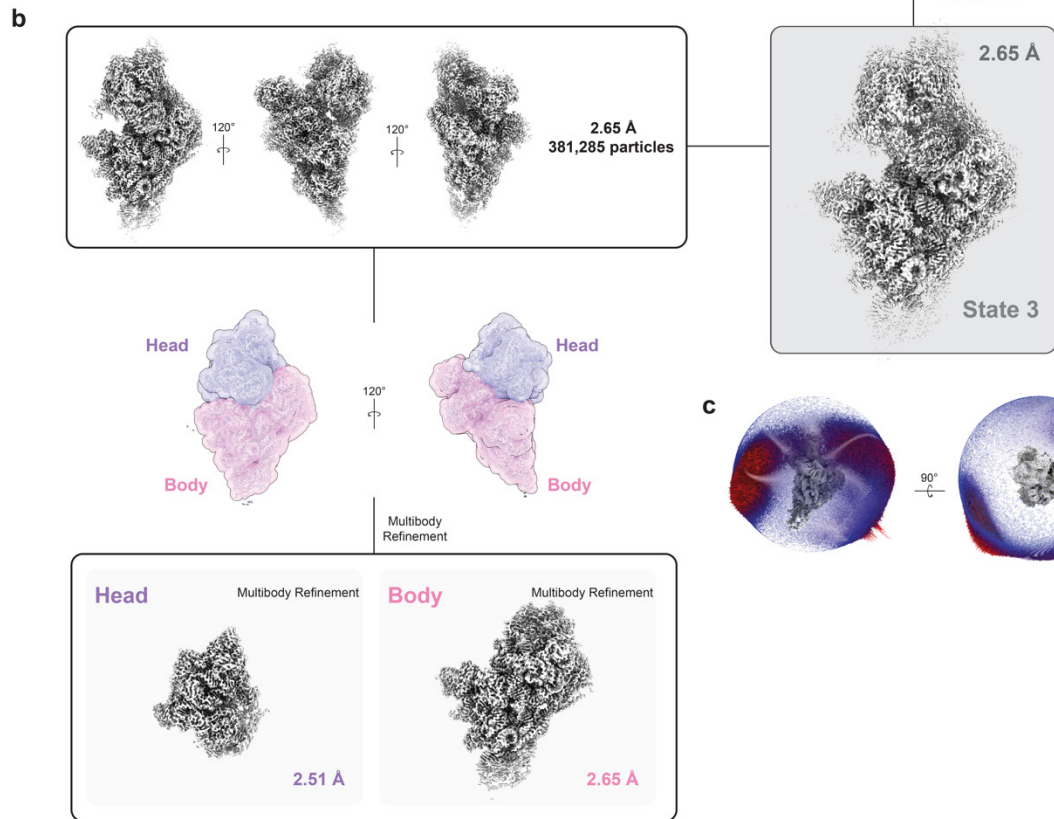
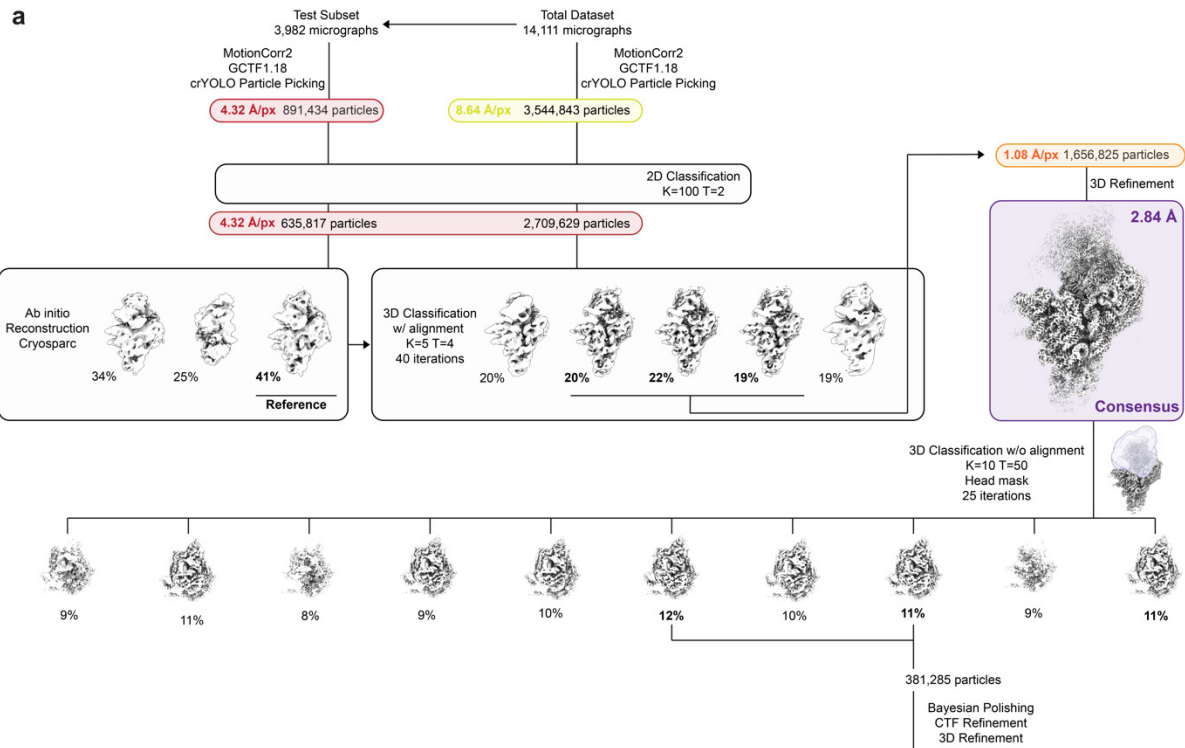
### State 2



**Supplementary Fig. 22. Cryo-EM processing of yeast States 1 and 2.**

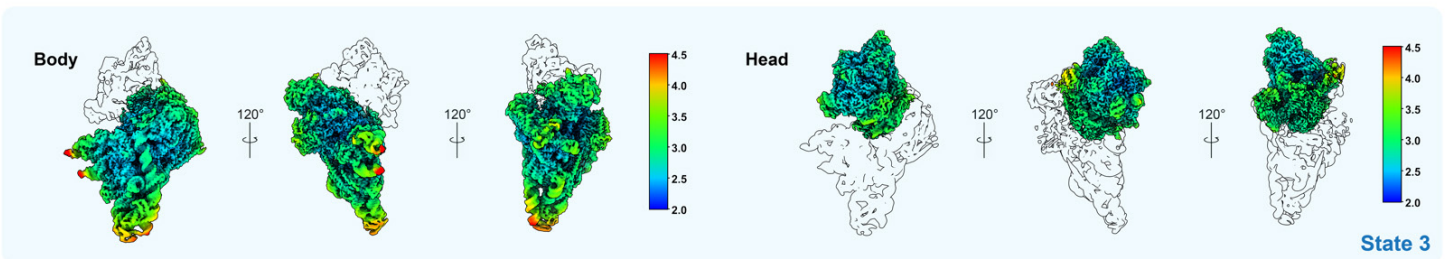
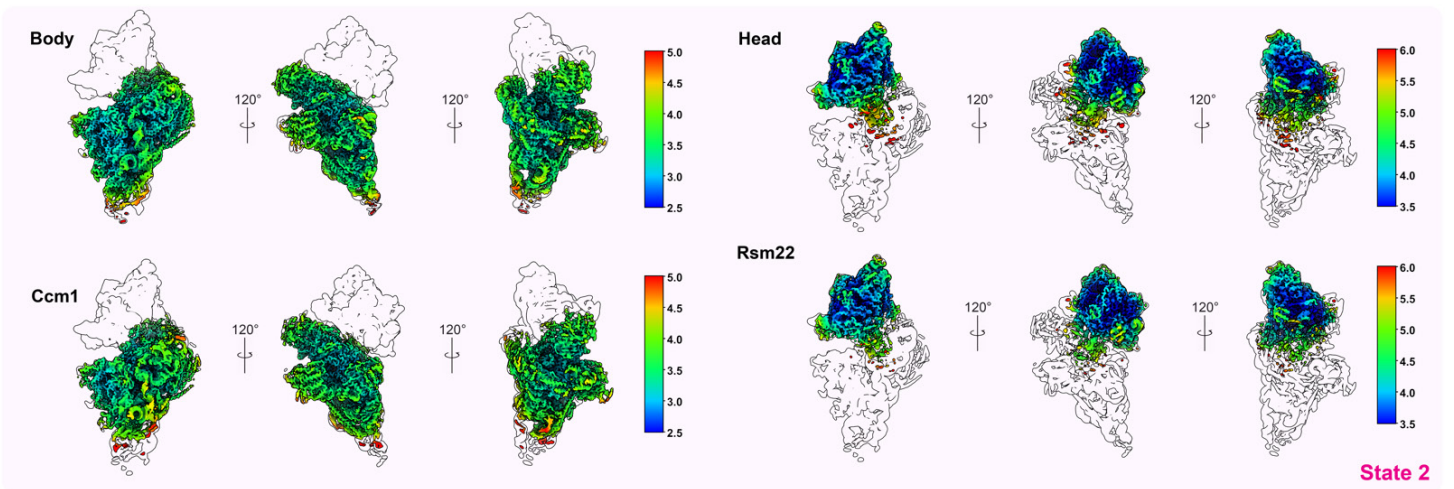
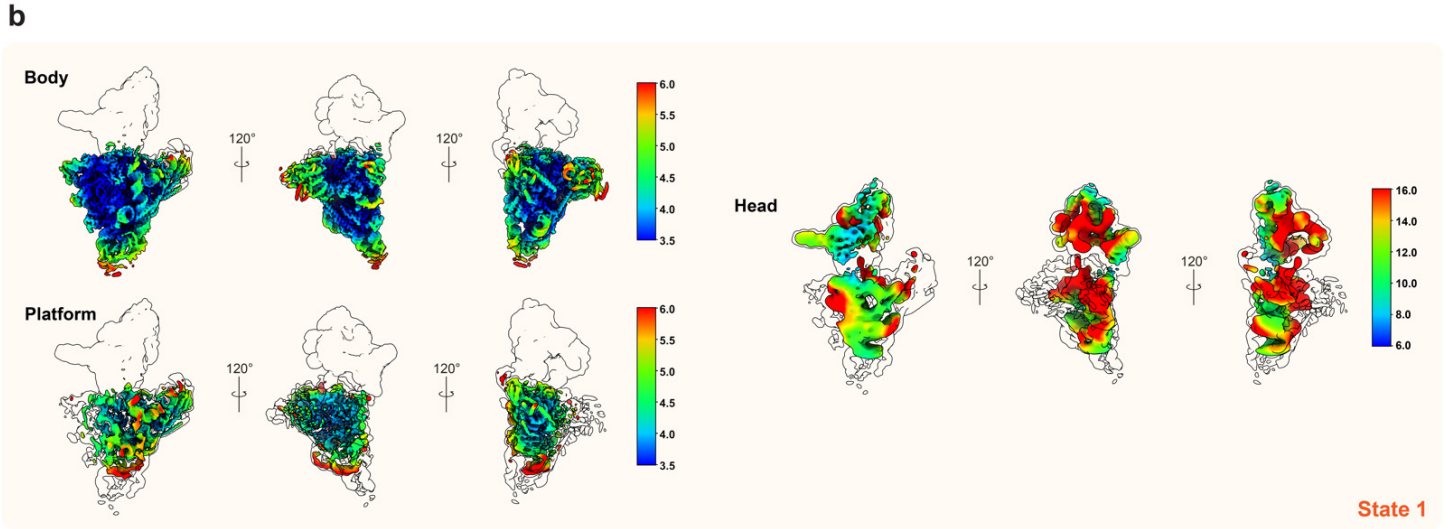
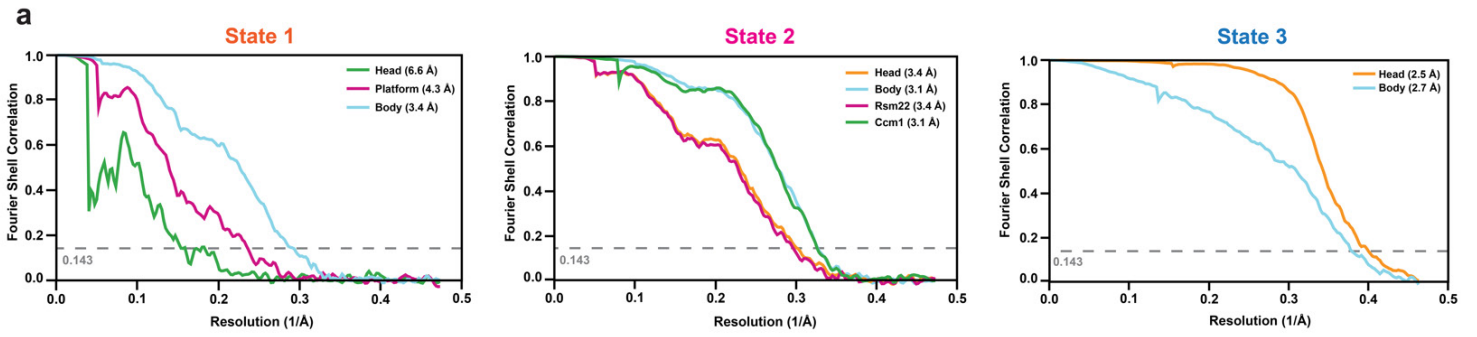
(a) Particles identified as State 1 were refined using a mask on the body domain. (b) Euler angle distribution of the overall (body) refinement for State 1. (c) Particles were classified using a mask on the platform and subsequently refined. (d) Classification of these particles on the head domain and Rsm22. (e) Particles identified as State 2 were refined using a mask on the body domain. (f) Euler angle distribution of the overall (body) refinement for State 2. (g) Particles were classified using a mask on Ccm1 and subsequently refined using a larger mask encompassing most of the body. (h) Particles were refined with a mask on the head domain and further classified. (i) To improve fragmented density corresponding to Rsm22, this region was subjected to an additional round of masked classification and refinement. Reported resolutions (FSC=0.143) from Relion post-processing are reported next to individual focused maps. Masks used are color coded.





**Supplementary Fig. 23. Cryo-EM processing of yeast Rsm22-containing particles (State 3).**

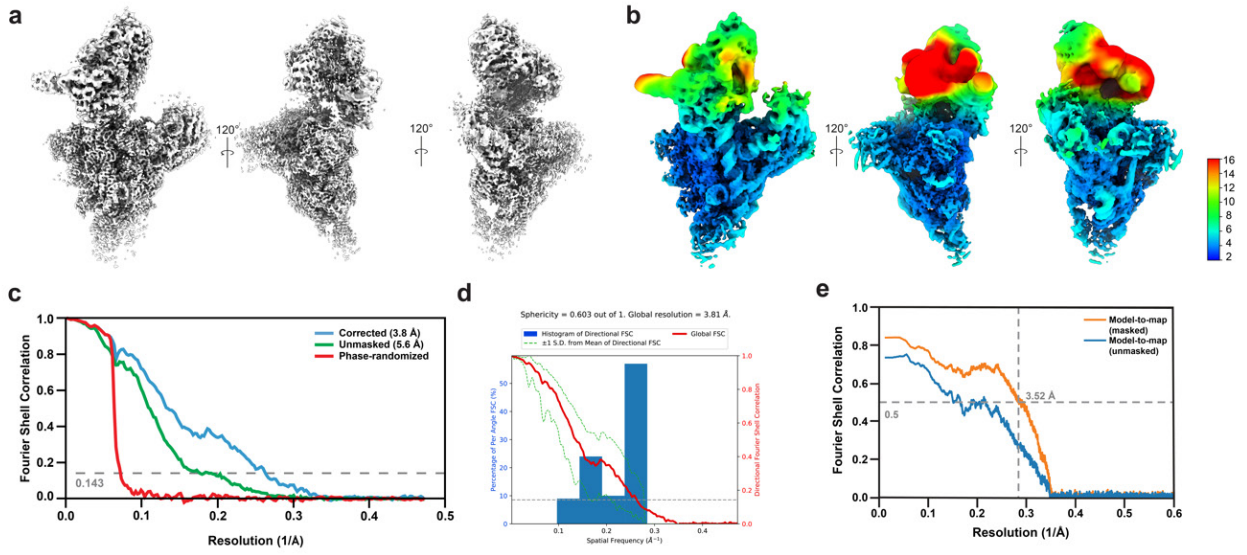
(a) Workflow for initial data processing to identify particles corresponding to State 3, resulting in a 2.65 Å consensus map. (b) Three views of the consensus map. The resolution of the head domain was improved using multibody refinement. (c) Euler angle distribution of the overall (body) refinement for State 3. Reported resolutions (FSC=0.143) from Relion post-processing are reported next to individual focused maps. Masks used are color coded.



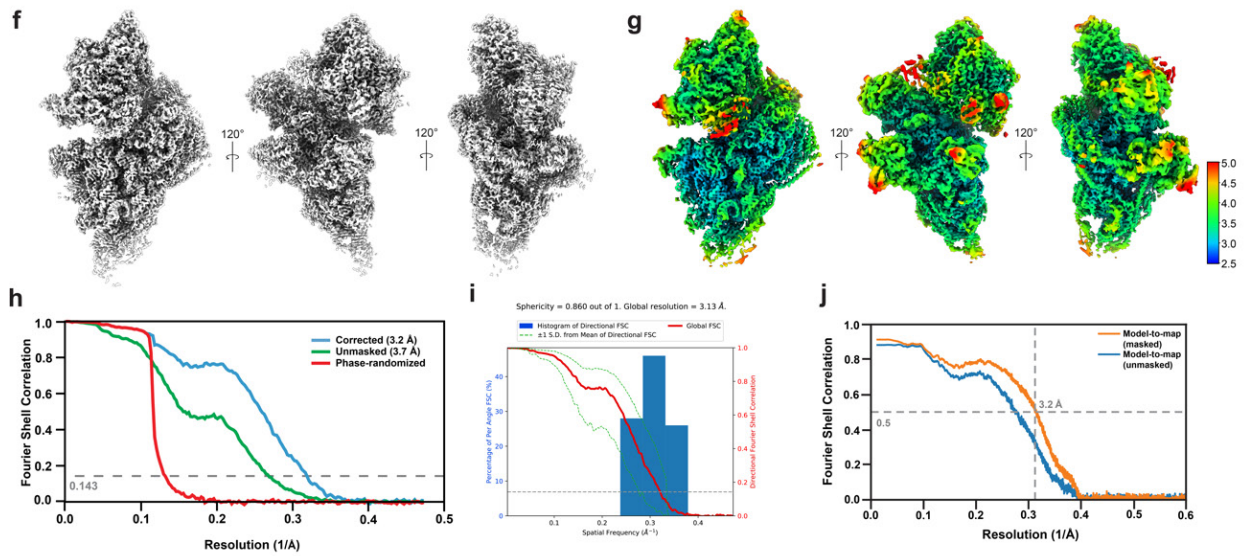
**Supplementary Fig. 24. Local resolution analysis of yeast reconstructions.**

(a) Solvent-corrected FSC curves for each focused refinement determined at FSC=0.143 via post-processing in Relion. (b) Local resolution estimation (calculated in Relion) for each focused map in context with the rest of the reconstruction.

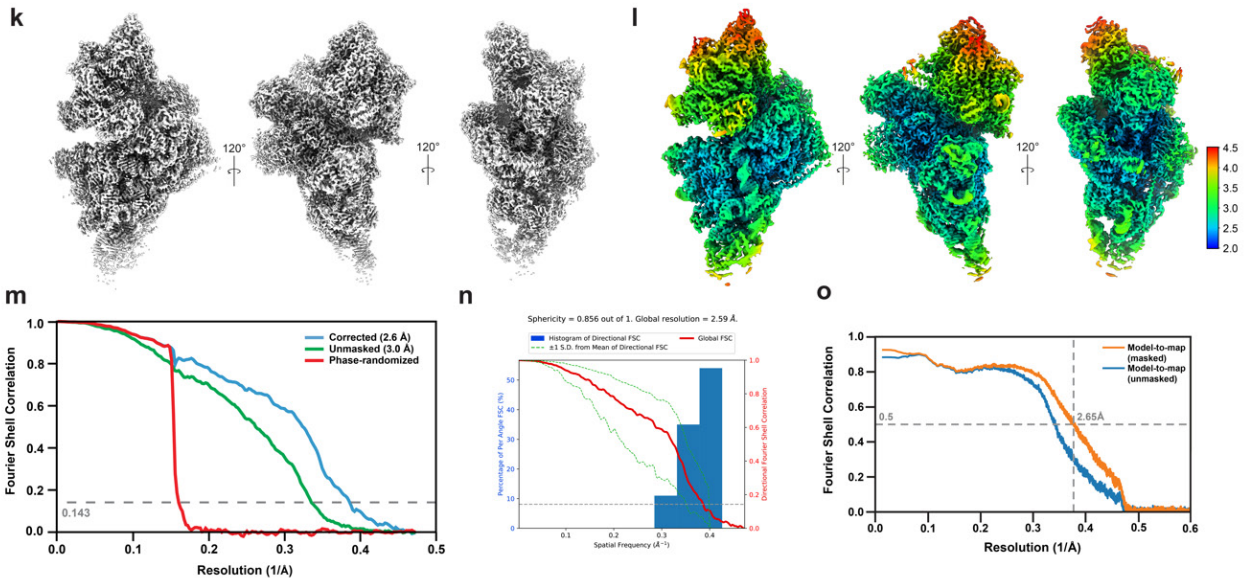
### State 1



### State 2

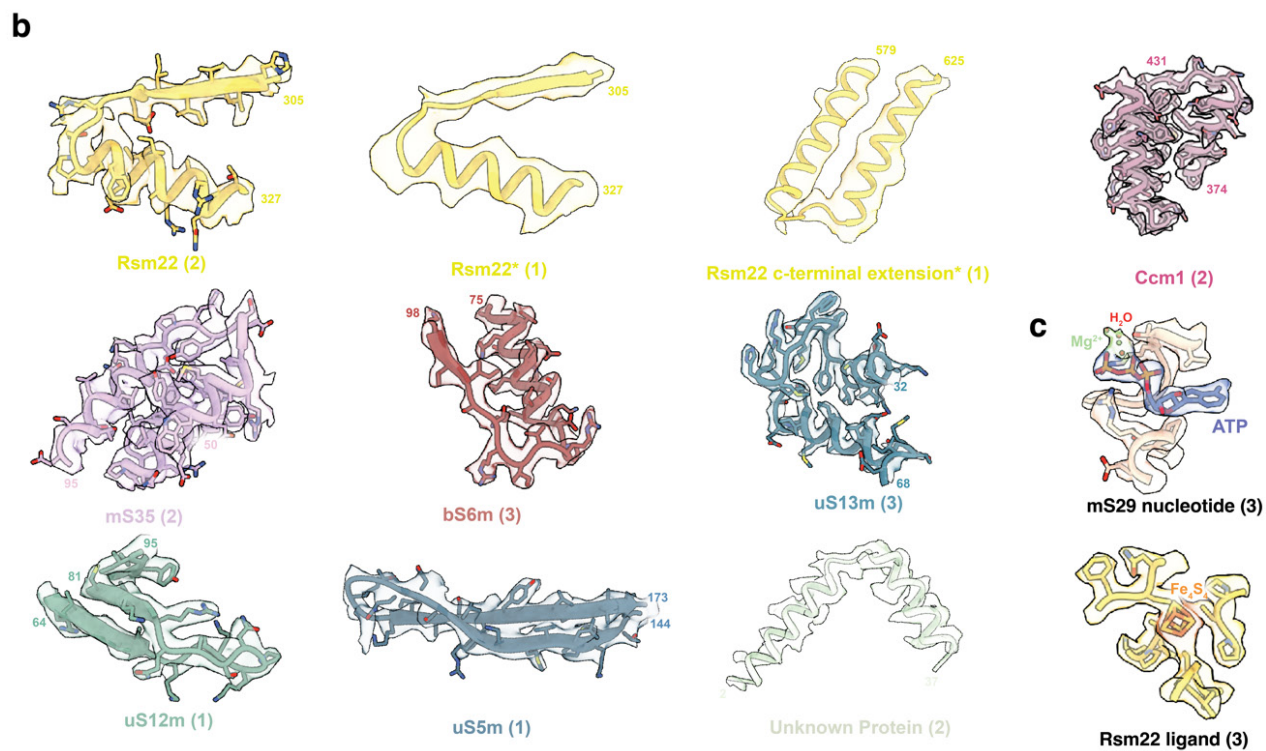
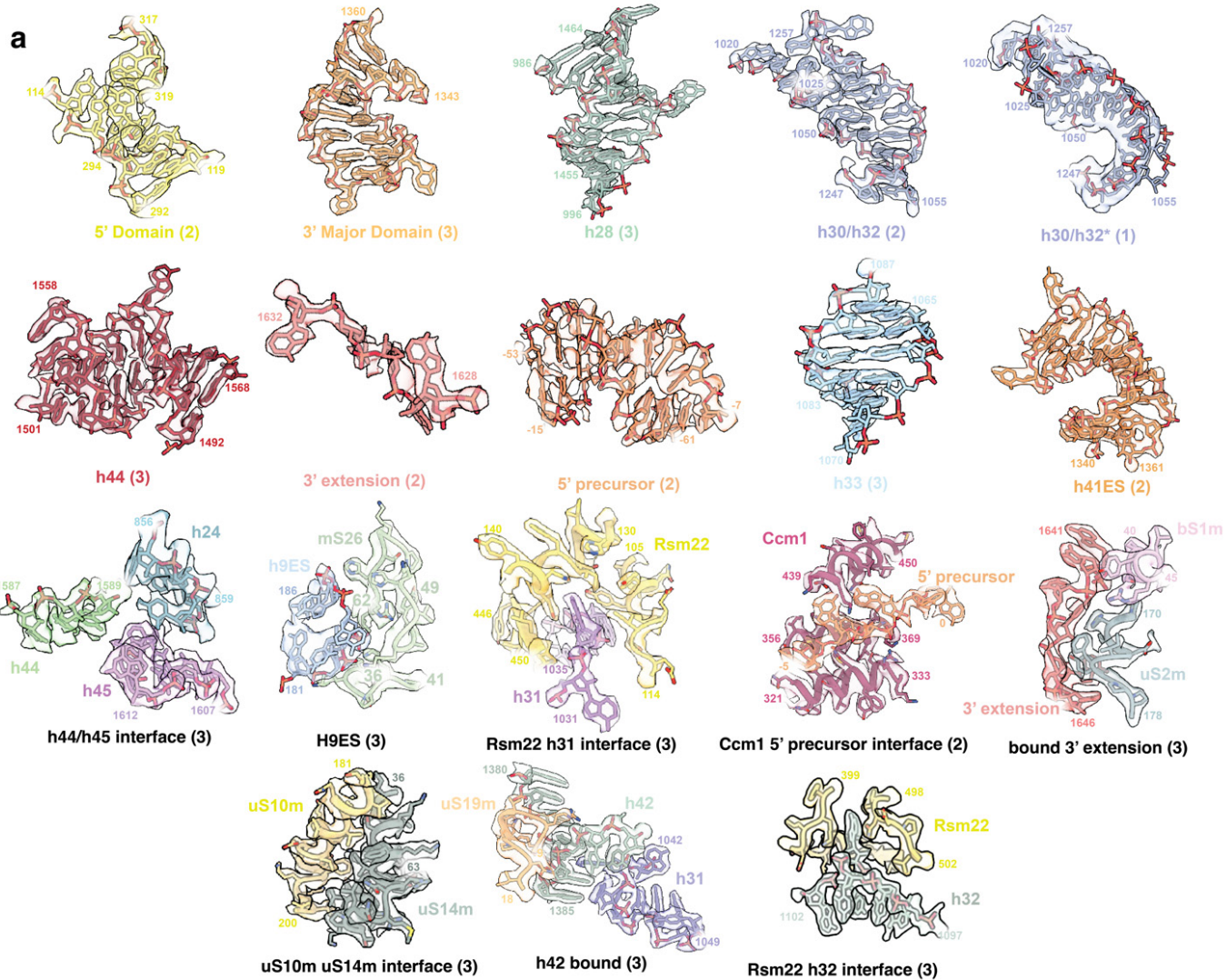


### State 3



**Supplementary Fig. 25. Validation of composite maps for yeast States 1-3.**

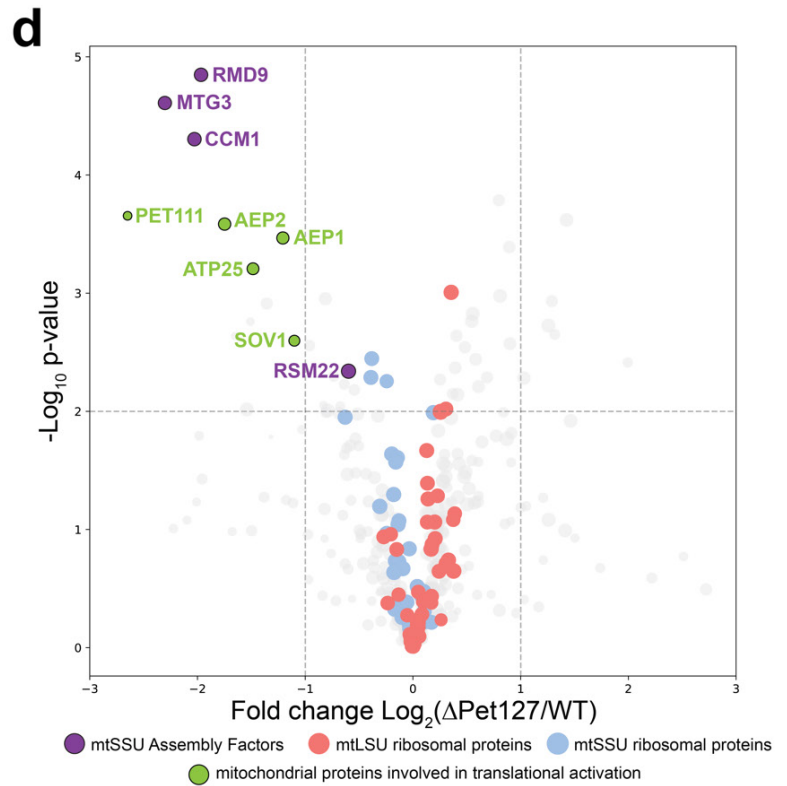
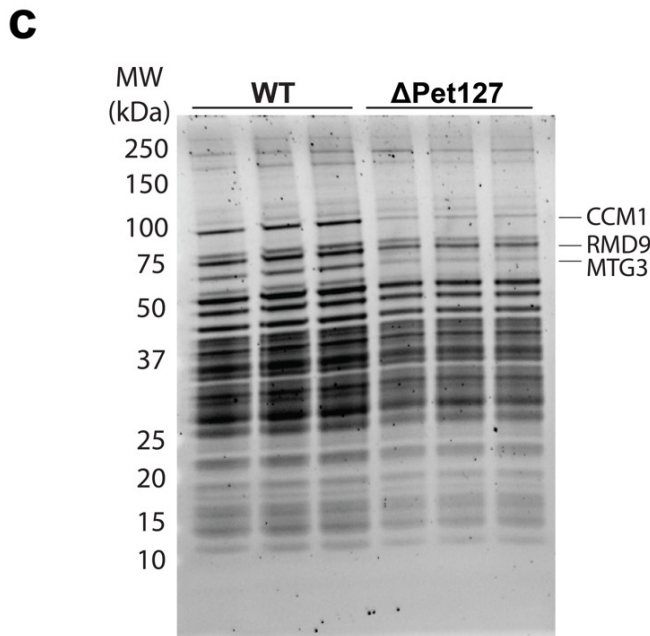
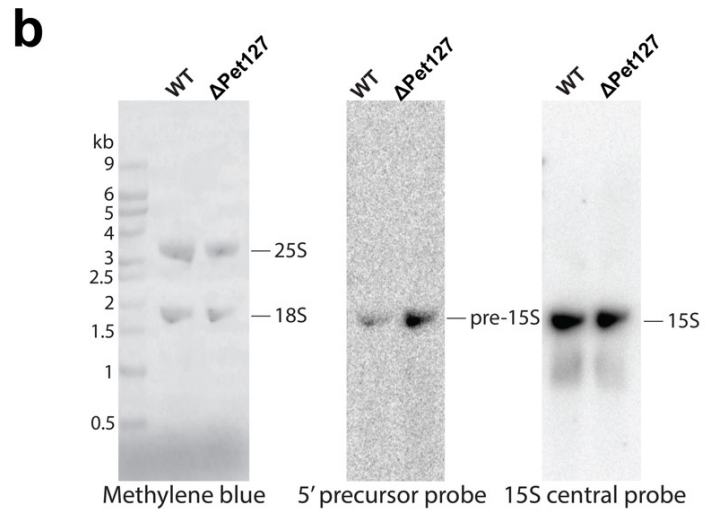
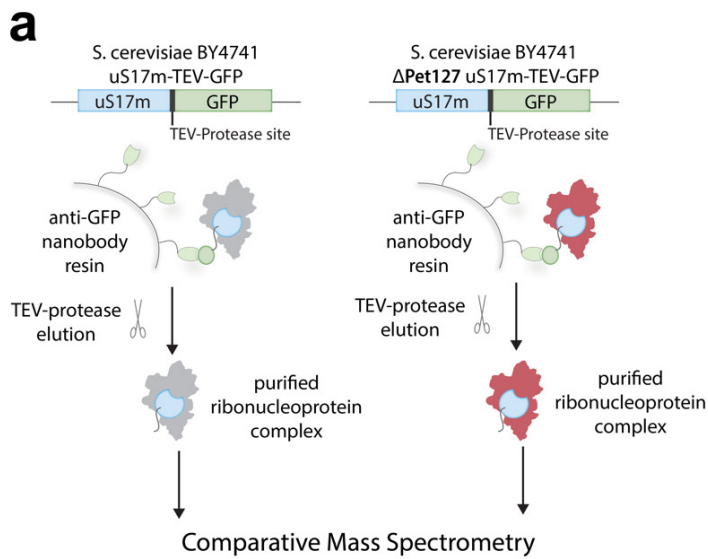
(a) Different views of the composite map of State 1. (b) Different views of the composite map of State 1 filtered and colored according to local resolution as calculated by cryoSPARC. (c) FSC curves for the State 1 composite map as calculated in Relion. Reported resolutions were determined at FSC=0.143. (d) 3DFSC for the State 1 composite map calculated using the Remote 3DFSC Processing Server<sup>1</sup>. (e) Map-to-model correlation between the State 1 composite map and the State 1 model. (f) Different views of the composite map of State 2. (g) Different views of the composite map of State 2 filtered and colored according to local resolution as calculated by cryoSPARC. (h) FSC curves for the State 2 composite map as calculated in Relion. Reported resolutions were determined at FSC=0.143. (i) 3DFSC for the State 2 composite map calculated using the Remote 3DFSC Processing Server<sup>1</sup>. (j) Map-to-model correlation between the State 2 composite map and the State 2 model. (k) Different views of the composite map of State 3. (l) Different views of the composite map of State 3 filtered and colored according to local resolution as calculated by cryoSPARC. (m) FSC curves for the State 3 composite map as calculated in Relion. Reported resolutions were determined at FSC=0.143. (n) 3DFSC for the State 3 composite map calculated using the Remote 3DFSC Processing Server<sup>1</sup>. (o) Map-to-model correlation between the State 3 composite map and the State 3 model.



**Supplementary Fig. 26. Representative cryo-EM densities and models for yeast structures.**

Selections of representative densities of RNA and protein across all states, comprised of (a) rRNA and functionally relevant protein-RNA and protein-protein interfaces, (b) assembly factors and mitoribosomal proteins, and (c) ligands. The states from which density and models are derived are shown in parenthesis below each panel, and \* denotes maps that have been filtered to local resolution.





**Supplementary Fig. 27 - Pet127 knockout results in accumulation of pre-15S rRNA and a decrease in bound assembly factors.**

(a) Experimental scheme for comparative IP-MS/MS in WT and PET127 KO yeast cells.

(b) Northern blots of extracted RNA after immunoprecipitation of uS17m-bound complexes. Northern blotting experiments were performed twice with similar results. (c)

SDS-PAGE gel of eluted complexes after uS17m pulldown in triplicate. Assembly factors identified by mass spectrometry that are significantly decreased in Pet127 KO samples are labeled. (d) Volcano plot for comparative IP-MS/MS of WT and PET127

KO cells using uS17m as bait. IP-MS/MS experiments were performed in triplicate for each condition (n=3 biologically independent experiments). A 2-sided student t-test was

used to determine p-values for changes in protein abundance between WT and PET127 KO mtSSU purification experiments. Individual proteins are shown as circles, with blue

circles indicating mtSSU proteins, orange circles indicating mtLSU proteins, green circles indicating proteins involved in translational activation, and purple circles

indicating mtSSU assembly factors. Raw data is available in Supplementary Data S5.

For gel source data, see Supplementary Fig. 1.

**SUPPLEMENTARY REFERENCES**

1. Tan, Y. Z. *et al.* Addressing preferred specimen orientation in single-particle cryo-EM through tilting. *Nat. Methods* **14**, 793–796 (2017).